University of North Dakota
UND Scholarly Commons

Theses and Dissertations | Theses, Dissertations, and Senior Projects

January 2018

# Enhancement Of Phoshorus Removal Via Bioretention Cells Amended With Low Cost Materials

Nick Lindstrom

Follow this and additional works at: https://commons.und.edu/theses

Recommended Citation
Lindstrom, Nick, "Enhancement Of Phoshorus Removal Via Bioretention Cells Amended With Low Cost Materials" (2018). *Theses and Dissertations*. 2272.
https://commons.und.edu/theses/2272

This Thesis is brought to you for free and open access by the Theses, Dissertations, and Senior Projects at UND Scholarly Commons. It has been accepted for inclusion in Theses and Dissertations by an authorized administrator of UND Scholarly Commons. For more information, please contact zeineb.yousif@library.und.edu.

# ENHANCEMENT OF PHOSPHORUS REMOVAL VIA BIORETENTION CELLS AMENDED WITH LOW COST MATERIALS

by

Nicholas E. Lindstrom

Bachelor of Science, University of North Dakota, 2016

A Thesis

Submitted to the Graduate Faculty

of the

University of North Dakota

In partial fulfillment of the requirements

For the degree of

MASTER OF SCIENCE

Grand Forks, North Dakota

August

2018

Copyright 2018 Nicholas E. Lindstrom

This thesis, submitted by Nicholas E. Lindstrom in partial fulfillment of the requirements for the Degree of Master of Science from the University of North Dakota, has been read by the Faculty Advisory Committee under whom the work has been done and is hereby approved.

Dr. Feng Xiao (Chair): _____

Dr. Sukvarsh Jerath: _____

Dr. Yeo Howe Lim: _____

This thesis is being submitted by the appointed advisory committee as having met all of the requirements of the School of Graduate Studies at the University of North Dakota and is hereby approved.

Dr. Grant McGimpsey: _____

Date: _____

| | |
|---|---|
| Title | Enhancement of Phosphorus Removal via Bioretention Cells Amended with Low Cost Materials |
| Department | Civil Engineering |
| Degree | Master of Science |

In presenting this thesis in partial fulfillment of the requirements for a graduate degree from the University of North Dakota, I agree that the library of this University shall make it freely available for inspection. I further agree that permission for extensive copying for scholarly purposes may be granted by the professor who supervised my thesis work or, in his absence, by the Chairperson of the department or the dean of the School of Graduate Studies. It is understood that any copying or publication or other use of this dissertation or part thereof for financial gain shall not be allowed without my written permission. It is also understood that due recognition shall be given to me and to the University of North Dakota in any scholarly use which may be made of any material in my thesis.

Name: Nicholas E. Lindstrom

Date: 04/03/2018

# Contents

# List of Figures

# List of Tables

# List of Abbreviations

| | |
|---|---|
| **WTR** | **W**ater **T**reatment **R**esidual |
| **LID** | **L**ow **I**mpact **D**evelopment |
| **BMP** | **B**est **M**anagement **P**ractice |
| **P** | **P**hosphorus |
| **GFWTP** | **G**rand **F**orks **W**ater **T**reatment **P**lant |
| **T.D.** | **T**reated **D**epth |
| **PP** | **P**articulate associated **P**hosphorus |
| **DP** | **D**issolved **P**hosphorus |
| **DOP** | **D**issolved **O**rganic **P**hosphorus |
| **SRP** | **S**oluble **R**eactive **P**hosphorus |
| **NOM** | **N**atural **O**rganic **M**atter |
| **rpm** | **r**evolutions **p**er **m**inute |
| **SE** | **S**tandard **E**rror of regression |
| **NTU** | **N**ephelometric **T**urbidity **U**nit |
| **ED** | **E**xhaustion **D**epth |

## ACKNOWLEDGEMENTS

I would like to extend my gratitude to my advisor and committee chair Dr. Feng "Frank" Xiao for his continuous support and assistance during this thesis as well as my time at the UND. I am also grateful to my committee members Dr. Sukhvarsh Jerath and Dr. Yeo Howe Lim for their advice and support during my time in the master's program at the University of North Dakota

**ABSTRACT**

As bioretention systems are becoming an increasingly popular low impact development (LID) application for stormwater mitigation, they lack mechanisms that demobilize phosphorus (P) especially dissolved phosphorus (DP). In many cases, these LIDs release more P than is input due to a high P index derived from the plant material inherent within bioretention systems. The objectives of this project are to utilize low-cost water treatment residuals (WTR) as bioretention amendments to capture P. The adsorption characteristics are observed by means of batch level experiments to observe the P adsorption potential without the influence of hydraulic parameters, and column experiments to observe P adsorption capacities more applicable to that in a bioretention column. Langmuir and Freundlich isotherm models were fit to the composite isotherms to determine the equation parameters and discover peak adsorption capacities. The Freundlich model better fit the $FeOH_3$ floc isotherms while the Langmuir model was more suitable for the $AlOH_3$ floc isotherms. The models output 7.114 mg- P/g and 1.390 mg-P/g for the $FeOH_3$ and $AlOH_3$ flocs respectively. The Thomas model was employed to the column experiment residual P data to discover peak adsorption capacities, were it computed 2.315 mg-P/g and 1.845 mg-P/g for the $FeOH_3$ and $AlOH_3$ flocs respectively. These adsorption values are similar to that of Geolithe and Hematite as indicated in literature.

The adsorption mechanisms primarily transpired by means of outer-sphere complexation. This mechanism rendered loosely bound P to the amendments permitting rapid, liable adsorption, but also left the adsorbed P susceptible to mild/moderate

desorption. Adsorption capacities were further inhibited by high pH levels and the presence of polymers in conjunction with the WTR. Overall, the WTR were successful in capturing DP in a wide variety of scenarios, validating their usage as an effective, low-cost, innovative solution in reducing phosphorus loading within bioretention systems.

# Chapter 1

# INTRODUCTION

## 1.1 Background

As an agricultural state, North Dakota purchases and employs approximately 257,300 tons of phosphorus (P)- fertilizers annually for growing crops (USEPA, 2011). P- fertilizers are also persistently used in lawns and gardens in rural and urban areas. Continuous use of conventional, highly soluble fertilizers, renders long-term detrimental effects on the soil fertility and water quality. Due to the lack of application efficiency, it has been estimated that 50 percent of conventional P- fertilizers applied to agricultural fields is not utilized by crops, but runs off with snowmelt and stormwater to nearby lakes and streams (Cordell, Drangert, & White, 2009). Loss of P from agricultural lands applied with conventional fertilizers not only results in negative agronomic and environmental consequences including decreased crop profitability and water impairment, it costs the state billions of dollars every year. P-limited lakes and rivers that become eutrophic, degrade water quality and destroy fish habitats, this water has little appeal for recreation; additionally, treatment costs increase if drinking water sources become eutrophic (Roy-Poirier, Champagne, & Filion, 2010). For these reasons, federal and state agricultural and water resources agencies face continuing challenges to manage P pollution in runoff and to minimize the adverse impacts of P discharge to water quality.

### 1.1.1 Need for Research

To reduce the discharge of runoff contaminates to receiving water bodies, many states including North Dakota implement stormwater best management practices (BMPs) to control and manage the quality and quantity of agricultural/urban runoff. Surface runoff and the associated negative effects can be controlled by various structural BMPs including detention basins, wet retention ponds, constructed wetlands, hydrodynamic separators, bioretention cells, and biofilters. While typical runoff treatment systems still consist of retention and detention ponds, many have started to use more localized and low-impact development (LID) techniques (i.e., bioretention cells and biofilters) to provide more integrated ecological and aesthetic benefits.

These LIDs can capture particle-associated phosphorus (PP) via settling and filtration in most stormwater treatment practices, but very few possess a mechanism that consistently captures dissolved phosphorus (DP) (Erickson, Gulliver, & Weiss, 2012); moreover, bioretention cells have been discovered to possess negative removal efficiencies of DP due to a high P index. Since DP constitutes a substantial fraction of P in stormwater, and more detrimental to ecosystems, LIDs/BMPs need to be better designed to remove dissolved nutrients. One such enhanced treatment strategy is to include a media with high P sorption capacity, such as sand amended with zero valent metallic compounds (Erickson et al. 2012). Zero valent metallic compounds can be purchased through a manufacturer or found in industrial wastes also known as by-products. Some waste materials that have been studied include: fly ash, blast furnace slag, red mud, spent alum sludge, and aluminum and iron rich water treatment residuals (WTR). These by-products when utilized as amendments, have a major advantage in that they are very cost effective (Zeng, Li, & Liu, 2003).

## 1.2 WTR project application

This project will utilize the aluminum and iron based WTR as amendments embedded within the bioretention media to immobilize DP from the stormwater by means of physical and chemical adsorption mechanisms. These materials are chosen because they are readily available at numerous water treatment plants around the country. The performance of these materials will be measured by strictly observing the adsorption potential in a batch reactor and then measuring the adsorption potential in a system replicating that of a bioretention cell.

# Chapter 2

# A LITERATURE REVIEW

## 2.1 Stormwater Nutrient Detriments

Eutrophication of water bodies in the United States has been recognized as an increasing environmental issue. Eutrophication is the process of destroying aquatic plant and animal life as a direct result of excessive nutrient input. Nutrients such as nitrogen and P stimulate algal growth in surface water runoff that can potentially lead to algal blooms, shift in dominant taxa, light limitation/ increased turbidity, excess organic carbon, environmental hypoxia, and toxin production. Cyanobacteria, or blue algea, are recognized to thrive under eutrophic conditions; they release toxins that have been responsible for chronic health effects causing death in animals and occasionally humans (Roy-Poirier et al. 2010). Although nutrients encompass manifestations of nitrogen and P, DP is often the limiting nutrient in fresh water systems due its high bioavailabity and integral contribution in the biological makeup in plants via building DNA and cell membrane (Erickson et al., 2011). The typical plant biomass contains 0.05 to 1.0 percent P by plant weight (Corbridge, 2000).

A study monitoring 635 storm events in California discovered the median fraction of DP to total phosphorus (TP) is 44 percent and observed median concentration of DP is 0.15 mg/L-P with a range of 0.10- 0.40 mg/L-P (LeFevre et al., 2015). Another

study discovered that dissolved manifestations of P in stormwater can constitute as high as 90 percent of TP in stormwater (Erickson et al. 2007). Sources of P in urban stormwater include lawn fertilizers, leaf litter, grass clippings, unfertilized soils, detergents, and rainfall. (Erickson et al., 2012). P- limited lakes and rivers that become eutrophic degrade water quality and destroy fish habitats, this water has little appeal for recreation; additionally, treatment costs increase if drinking water sources become eutrophic (Roy-Poirier et, al. 2010). BMPs preceding lakes and rivers need to be better suited to protect these sensitive water bodies from excessive nutrient input.

### 2.1.1 Need for BMP Innovation

Only select studies have focused on DP removal in bioretention and its fate is fairly unknown within the bioretention system. Particle-associated phosphorus (PP) can be captured via settling and filtration in most stormwater treatment practices, but very few practices have a mechanism that consistently captures DP (Erickson et al., 2012). However, since DP constitutes a substantial fraction of phosphorus in stormwater (as mentioned above), and more detrimental to ecosystems, BMPs need to be better designed to remove dissolved nutrients. Figure 2.1 illustrates the P and DP removal efficiencies of five popular BMPs collected from the International Stormwater BMP database. There is hardly any statistically significant data to show these BMPs remove P, especially DP. Matter of fact, there is a vivid negative DP removal efficiency performed by bioretention and its biofilter counterpart. Despite the poor P removal efficiency of bioretention systems, they are becoming increasingly popular in LID designs because they have proven to provide effective at-source stormwater retention, peak flow attenuation, and pollutant removal (Davis, Hunt,Traver, & Clar, 2009). They also

improve the aesthetics of the employed LID, are relatively inexpensive to install and maintain, and typically small in size ( Davis et al., 2009).

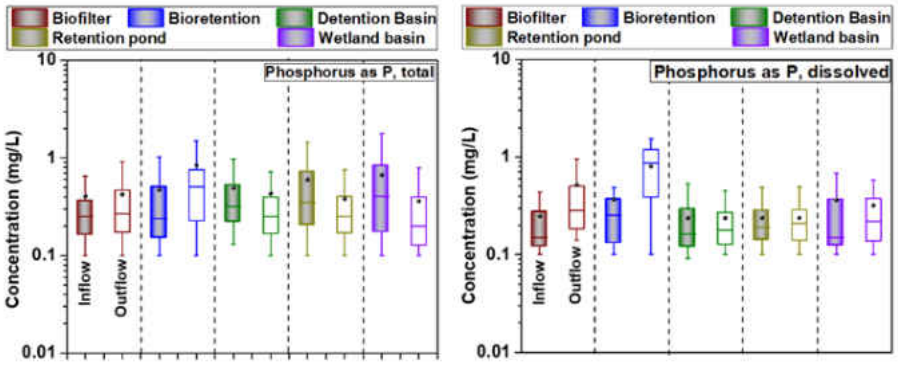


FIGURE 2.1: Inflow and outflow concentrations of P (DP, TP) of various BMPs obtained by the International BMP Database

To render a bioretention system configuration that has the capabilities of removal and or transformation of DP, multivalent metallic amendments should be added that possess the capabilities of adsorption, precipitation, ion exchange, and biological processes (Davis et al. 2009). To possess a better understanding of how these amendments should be implemented within a bioretention cell, the bioretention hydraulic, chemical, and biological characteristics need to be comprehended.

## 2.2 Bioretention System Overview

Structural BMPs, such as bioretention systems, are designed to function without human intervention at the time wet weather flow is occurring, thus are expected to function unattended during a storm and to provide passive treatment. This project will

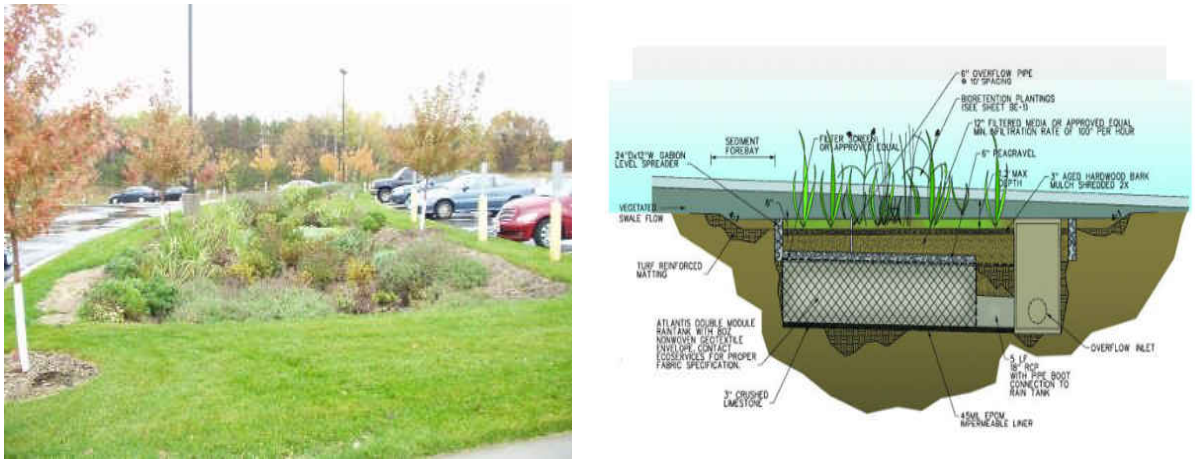


(A) (B)

FIGURE 2.2: (A): Bioretention cell employed in a parking lot. (B): profile view of a typical bioretention cell.

focus on one popular structural BMP, bioretention (also called rain gardens; see Figure 2.2). Bioretention is one of the most popular LIDs used in urbanized watersheds since the early 1990s (Roy-Poirier et al. 2010). Bioretention cells are shallow vegetated depressions containing an engineered soil media into which stormwater from impervious surfaces is directed for infiltration (Davis, & McCuen, 2005). The infiltrated water may be collected by an underdrain and discharged into a surface water body or simply allowed to percolate to underlying groundwater. These systems treat stormwater via a range of chemical, physical, and biological processes which incorporate mechanical filtration, sedimentation, adsorption, and plant and microbial uptake and have been substantially proven to reduce peak flows, runoff volumes, and pollutant loads (Lucke, 2015). Despite the rapid acceptance of this BMP practice, there lacks detailed information pertaining to many of the biological and chemical design parameters for different regions of the states.Like other structural BMPs, conventional bioretention is inefficient towards the removal of P, especially DP.

Developing a bioretention system that effectively removes DP is not an easy task. Bioretention incorporates many mechanisms that create a complex environment for P. Kinetics equilibrium, solubility, speciation, etc. of DP in bioretention will all contribute to the effectiveness of DP removal within the system. The next section will address the general DP speciation and its interaction with bioretenion media and it's amendments.

## 2.3 General Properties of P and Bioretention Removal Mechanisms

P in agricultural/urban runoff rarely exists as its elemental state, it is distributed between DP forms and P associated with particulate matter (PP). According to a California study, a sample size of 635 storm events discovered that the DP concentration in the runoff ranged from 0.01 – 2.4 mg-P/L ( median = 0.06) (Kayhanian, Suverkropp, Ruby, & Tsay, 2007) and the fraction of DP to TP was 44 percent (maestre, & Pitt, 2005). DP is more mobile, bioavailable, and captured via different mechanisms that particulate P. DP can be separated further into dissolved organic phosphorus (DOP) and soluble reactive phosphorus (SRP) also known as orthophosphate ($H_xPO_4^{3-x}$) (Stumm, & Morgan, 1981). Albeit DOP may become bioavailable for plant and animal uptake by microbial action, it will not contribute to eutrophication until it is converted. Bioretention with a low P index will have a trace amount of this DOP with the majority of its concern surrounding SRP. SRP is more concerning because of its immediate bioavailability and complimentary harmful effects to the receiving waters as discussed previously. SRP speciation is strictly dependent on the pH as demonstrated in Figure 2.3 and Table A.1 (see Appendix A).

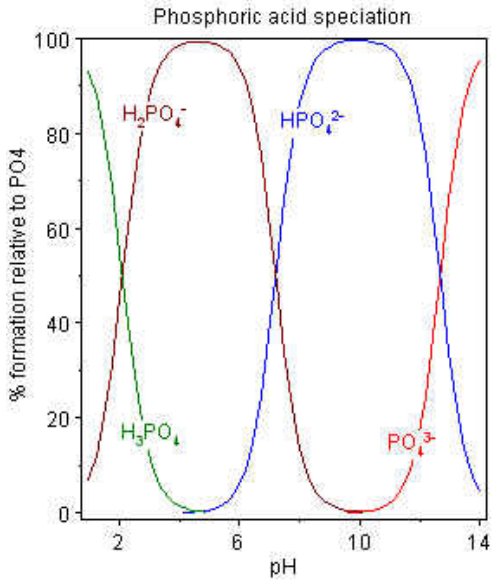


FIGURE 2.3: SRP ionization fraction at 25 °C

In natural waters (pH: 6-8) SRP will exist primarily as $H_2PO_4^-$ and secondarily as $HPO_4^{2-}$. The speciation of DP in a bioretention system plays a critical role in how effectively the removal mechanisms will perform. Since The primary role of DP will be SRP in respect to this project, SRP will only be referred to DP for future reference. Figure 2.4 is a visual summary of the P cycle mobilization/ immobilization processes in a bioretention system. Not only will pH control the speciation of DP, it enables other driving mechanisms that assists DP removal. One of those mechanisms is adsorption, which is believed to possess the most capacity to remove DP in bioretention at the pertinent pH.

### 2.3.1 Sorption/Desorption Mechanisms

Sorption is believed to be the major contributor of DP removal in bioretention systems. Sorption consists of a chemical and physical process by which a substrate becomes

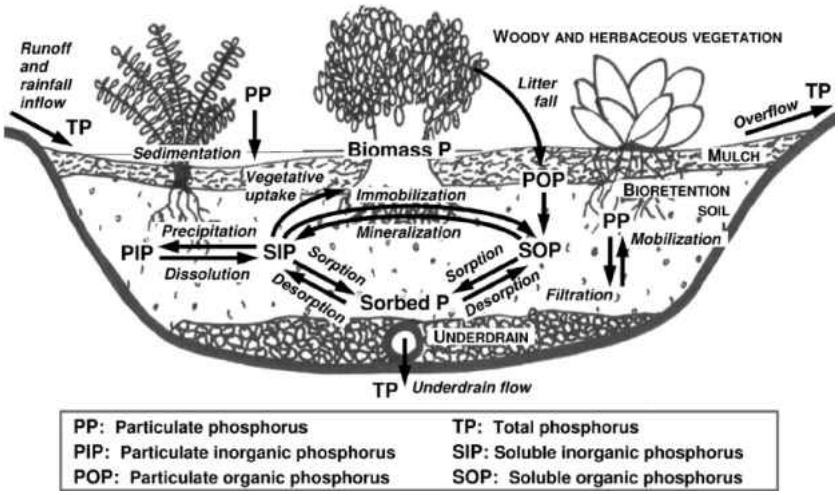


FIGURE 2.4: Profile view of the mobilization/immobilization processes of P within a bioretention system. Image borrowed from (Roy-Poirier, 2010)

attached to a adsorbent. It encompasses both absorption and adsorption processes. Adsorption is a surface phenomenon in which surface adhesion of atoms, ions, or molecules from gas, liquid, or dissolved solid to a surface occur. This process creates a film of the adsorbate (DP) on the surface of the adsorbent. This process differs from absorption, in which a substance is dissolved by or permeates the bulk phase of a material (the absorbent). Namely, adsorption is a surface-based process while absorption is a sub-surface based. Similar to surface tension, adsorption is a consequence of surface energy. In a bulk material, all the bonding requirements ( ionic, covalent, or metallic) of the constituent atoms of the material are filled by other atoms in the material. The adsorption process is generally classified as a physisoption (characteristic of van der wall forces), chemisorption (covalent bonding), and ion exchange process were the type of adsorption depends upon the binding energy of the substrate. Physisorption is acknowledged to be the most prominent adsorption process in the adhesion of P onto floc material due to the induced dipole interaction between the adsorbate and the adsorbent.

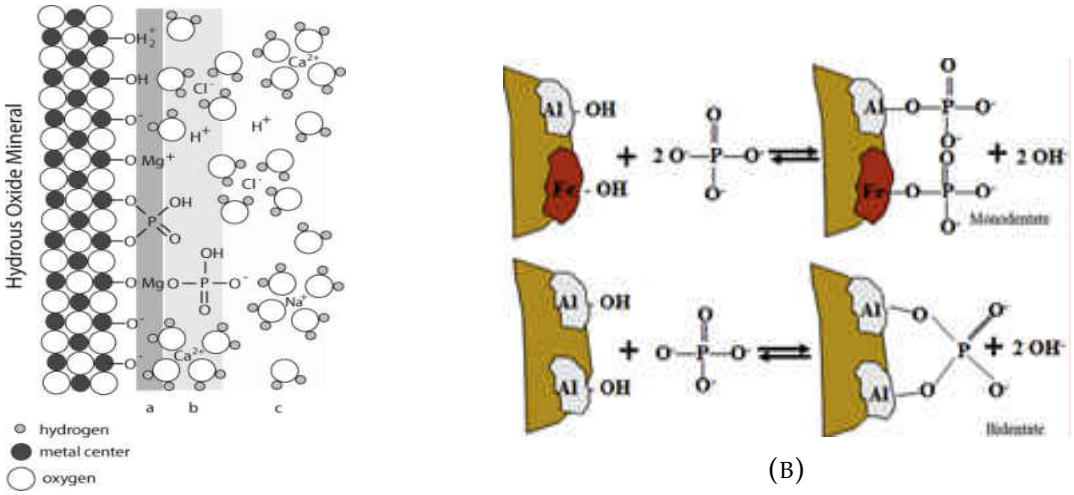


(A) (B)

FIGURE 2.5: (A): Inner and outer surface complexation with hydrous oxide mineral (Stewart et al. 2011). (B): The principles of P adsorption (inner sphere) onto AL and Fe (hydr)oxides. Image borrowed from (Li & Davis, 2015)

Metals such as aluminum and iron have strong affinities to enhancing the adhesion of DP and other dissolved nutrients to the soil amendments. DP also can be sorbed onto mulch and bioretention soil particles, while the capacity of a soil to sorb DP varies greatly depending on the organic and clay contents of the soil, presence of transition metals, and pH levels in the media (Roy-Poirier et al. 2010). Adsorption involves two types of reactions: fast, reversible attributed to outer sphere complexes by means of van der Waal forces following slower adsoprtion forming monodentate complexes. While Monodentate complex formation with the amendments are slower than the ion exchange reaction, it is still regarded as liable (Li & Davis, 2015). Slower irreversible reactions involves inner sphere complexation of ligands such as (hydr)oxides and orthophoshates which may take place over months (Bolan, 1991). Figure 2.5 illustrates the inner and outer adsorption processes.Kinetics experiments can verify what adsorption type is likely to occur based on the rate at which DP is removed from solution.

### 2.3.2 Chemical Precipitation of DP

DP precipitation is a slow, irreverable process usually with metallic ions such as the Al and Fe species in this case. DP can also bind with calcium and magnesium ions; however precipitation of DP is not the predominant removal mechanism because of the short residence time treated runoff has in the BMP and the corresponding short contact times with the amendments.The contact of DP with iron oxides and other metallic amendments are considered fast reversible reactions and highly pH dependent (Lefevre et al., 2015), therefore the kinetics should be considered in the reactions to determine the potential P adsorbed/precipitated. A kinetics experiment conducted in the lab demonstrated how quickly DP adsorbed onto alum flocs (Figure 2.6). Figure 2.6 illustrates the DP output concentration vs. time in a batch adsorption study suggesting the output concentration varied less than 5 percent over a 15 minute time span, indicating very liable sorption conditions (fast reactions). Similar results were produced for DP removal by alum floc at 60 mg/L located in Appendix A.

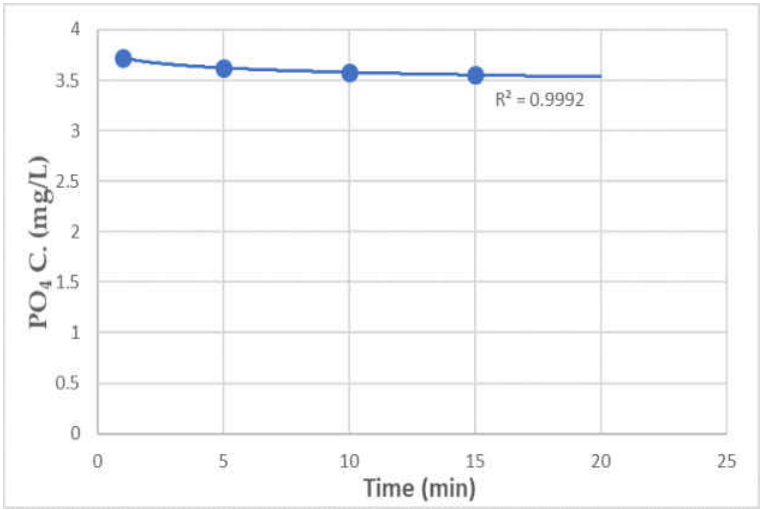


FIGURE 2.6: Phosphate adsorption kinetics. S= 0.0284 $R^2$= 0.9673, P= 0.002

The assumption can be made that a contact time of a minute or less will have the same removal efficiency as a contact time of 15 minutes. This is critical information because the treatable water will only have so much contact with the amendments in the BMP. The time of contact is limited in bioretention cells because they are designed to drain quickly to limit anoxic conditions and prevent ponding amongst other reasons, causing a potential limited sorption/precipitation capacity of the bioretention media (Roy-Poirier, et al. 2010).

## 2.4 Hypothesis

Removal of P especially DP can be greatly improved in biorentention cells by amending with low-cost, iron and aluminum based WTR. This approach may also be applied to other popular BMPs, including biofilters (swales and strips). The enhanced bioretention cells are expected to effectively capture P runoff of snowmelt and rainfall to surface water, thus protecting the water resources.

# Chapter 3

# EXPERIMENTAL PROCEDURES AND METHODOLOGIES

## 3.1 Scope and Objectives of Proposed Research

The major scope of this project is to investigate the performance of a novel, WTR amended bioretention system enhanced for the removal of P, especially DP. Two low-cost amendments, aluminum hydroxide floc and ferric hydroxide floc generated in the laboratory along with WTP floc collected from GFWTP will be analyzed and compared with literature studies. The specific objectives are to 1) study the adsorption of P on the adsorbents (aluminum hydroxide floc, and ferric hydroxide floc) in batch adsorption studies; and 2) investigate the removal of P in a simulated bioretention cells amended with adsorbents.

## 3.2 Batch Adsorption Experiment Procedure and Methodology

The following description is the basic experimental procedure for a batch adsorption analysis. Batch adsorption tests are conducted in a PB-700 Jar Tester where the coagulants are flocculated and the P stock solution is spiked. Distilled and/or surface water

obtained from the Red River of the North is used as the coagulation solution. $NaHCO_3$ is applied to distilled water to accommodate the consumption of alkalinity during the coagulation process; on the other hand, surface water possesses enough naturally alkalinity and has a higher pH for coagulation/flocculation to transpire on its own. Each jar sequentially increases the coagulant dosage ranging from 0 mg/L to 100 mg/L of coagulant (amendments). 1g/L - $PO_4$ stock solution is spiked at various dosages into the batch reactors, stirred for 10 minutes and settled for 15 minutes. A volumetric pipette (TD, $\pm$ .06 mL) extracts 25 mL of solute where it is filtered with a .45 $\mu$M filter paper by a vacuum pump. $PO_4$ is complexed by PHosVer 3 phosphate reagant and measured using a HACH DR/2000 Spectrophotometer.Batch adsorption experiments vary upon the mission/purpose of the experiment. The following sections explain The specific batch reactor experiment procedures and their methodology.

### 3.2.1 Organic Adsorption Experiment

The organics batch test compounds will include, IHSS Suwannee River 2S101H Humic acid, 2S101F Fulvic acid, and natural organic matter (NOM) found in surface water obtained from the Red River of the North. Adsorption isotherms will be constructed in batch reactors at concentrations ranging from near the instrumental quantification limit to about half water solubility. Because each point on the adsorption isotherm must be treated statistically as a separate datum, concentration replication will not be employed, but rather data (minimum of 18) will be spread out evenly over the isotherm on the log scale. 50 mL solute containing 0.66 $PO_4 - P$ mg /L and there respective doses of NOM is added to the vials containing 0.0550 g of dried $AlOH_3$ floc. Solute(s) will be tumbled gently at 25 °C for an appropriate time to reach the equilibrium as

determined in adsorption-kinetic experiments. The vials will be sealed with a PTFE-lined silicone rubber septum screw cap. The liquid phase will be deionized water containing 0.2 mmol/L $NaHCO_3$ to adjust the alkalinity upon adsorption. The pH of the solution is approximately 7.5. The effects of pH (adjusted by $NaHCO_3$) and ionic strength (adjusted by NaCl) will be examined, though it is unlikely that pH (6-8) and ionic strength (< 5 mmol/L) have significant effects on the adsorption of NOM.

### 3.2.2 Turbidity Effects on the Adsorption Experiment and Methodology

Similar to the standard adsorption batch experiments aforementioned, the P experimental procedure is the same. However "Swetha clay" is added at varying intervals to observe the effects of turbidity on the adsorption of $PO_4$ on WTR. The clay is added at 0.01 g intervals following coagulation and flocculation at a 60 mg/L alum dosage. Clay is added ensuing coagulation because floc would have exhibited different properties and impacted the P adsorption. The turbidity of each sample is measured following the test completion and samples are extracted while the jars are stirred at 150 rpm to ensure complete mixing.

## 3.3 Batch Adsorption Analysis Methodology

Adsorbed concentrations ($C_s$) will be calculated by mass balance. Adsorbent-free controls will run to automatically correct for bottle losses. Adsorption isotherms will be fit to the Freundlich model Eq.(3.1) or the Langmuir model Eq.(3.1):

$$C_s = K_F C_W^n \tag{3.1}$$

$$C_s = \frac{S_{LM} K_L C_W}{1 + K_L C_W} \tag{3.2}$$

Where $C_s$ and $C_w$ are the adsorbed and aqueous-phase concentrations, respectively. In Eq. (3.1), n is the Freundlich exponent providing an indication of isotherm non-linearity, and $K_F$ is the Freundlich adsorption coefficient, they will be obtained by linear least-weighted by the dependent variable. In Eq. (3.2), $S_{LM}$ and $K_L$ are the Langmuir maximum capacity and affinity coefficients, respectively, obtained by non-linear regression of experimental data weighted variable. The adjusted (degrees of freedom) coefficient of determination $R^2$ and standard error of regression (SE) will be computed and employed to compare fitting performance.The observed (concentration-dependent) distribution ratio $K_d$ is defined as the adsorbed-to-solution concentration ratio,

$$K_d = \frac{C_s}{C_W} \tag{3.3}$$

## 3.4 Column Experiments and Methodology

Continuous-flow column experiments will be conducted to generate P breakthrough curve as a function of active media and treated depth (TD) in a similar approach reported previously. Briefly, 10, 2.60 cm inside diameter columns, will be made from

clear PVC pipe sections. The length of each column is approximately 15 cm. The columns consisted of approximately 1 cm of gravel sub base at the bottom. Multiple columns will be prepared with differing ratios of active media to sand which cannot be predetermined due to the difficulty in weighing the amorphous floc mass. In addition, a single 100% sand column will be prepared to serve as a control. Compaction of the bioretention media will be done by carefully pounding on the column wall while slowly adding the media using a funnel. Peristaltic pumps will be used to pump synthetic stormwater from an influent reservoir into the bottom of the columns. The columns will be operated in an upflow mode to ensure saturation of the bioretention media and minimize the risk of short circuiting. The hydraulic loading rate will be around 10.0 ml/min $\pm$ 2.0, which will be monitored daily and adjusted if necessary. The effluents from each column will be collected in separate 3.8 L (1 gallon) jar so that the volume of water passed through the individual columns will be monitored. Aqueous samples will be collected periodically from the influent reservoir and the effluent of a column. A volumetric pipette (TD, $\pm$ .06 mL) extracts 25 mL of solute where it is filtered with a .45 $\mu$M filter paper by a vacuum pump. $PO_4$ is complexed by PhosVer 3 phosphate reagent and measured using a HACH DR/2000 Spectrophotometer.

### 3.4.1 Analysis Methodology

Two approaches will be used to estimate the bioretention media $PO_4 - P$ sorption capacities in the column experiments. First, a mass balance calculation similar to that used by (Davis et al., 2001) will be performed using the aqueous $PO_4 - P$ concentration data:

$$q = \frac{1}{X}\int_{0}^{V_eff} \left(C_{in} - C_{eff}\right) dV \tag{3.4}$$

where $C_{in}$ and $C_{eff}$ are influent and effluent PO4-P concentrations, respectively; X, mass of bioretention media; and $V_e$ff, cumulative effluent water volume at full $PO_4 - P$ exhaustion. Mass balance calculations will be performed on each column individually, and the mean sorption capacity will be computed for columns with similar TD. Second, effluent $PO_4 - P$ concentration data will fit, through nonlinear least squares regression, to the Thomas model:

$$\frac{C_{in}}{C_{eff}} = \frac{1}{1 + e^{\frac{k_{TH}}{Q}(qX - C_{in}V_{eff})}} \tag{3.5}$$

where $k_{TH}$ is the Thomas rate constant (mL/mg/min), q is the Thomas sorption capacity, Q is the flow rate through the column, and other parameters have been defined above. To obtain $PO_4 - P$ sorption capacities for the active media, the q value obtained from Eq. (3.4) will be corrected for sorption due to the intermediate sand layers using the sorption capacity of sand ($q_{ac}$) obtained from the sand-only column.

$$q_{ac} = \frac{qX - q_{sand}X_{sand}}{X_{ac}} \tag{3.6}$$

The $q_{ac}$, batch values determined from the batch sorption experiments will used to evaluate the sorption capacity of active media at equilibrium, whereas the $q_{ac}$ column values obtained from the column experiments will be used to determine the sorption capacity under continuous/non-equilibrium flow conditions. If the sand only column does not have any sorption capacity, Eq. (3.6) will be obsolete.

# Chapter 4

# DATA COLLECTION: COAGULATION MATRIX DISCUSSION

## 4.1 Overview

Truly, utilizing synthetic stormwater as the adsorption solution would minimize the influence of unknown constituents within the solution matrix. However, synthetic stormwater is only implemented a handful of times in the batch and column experiments because coagulation renders small/weak floc in the absence of turbidity; secondly, the floc products do not realistically characterize the water treatment plant floc products. Surface water provides that natural turbidity to create robust floc particles, unfortunately, it is also accompanied with the other constituents in its matrix which may significantly alter the adsorption capacity of the WTR. Potential substrate responsible for an influence of WTR adsorption capacity include but are not limited to: Calcium and magnesium compounds, turbidity levels, pH, temperature, and other negatively charged substrates like arsenic and NOM. These parameters may compete with P for adsorption sites, alter the adsorption kinetics, change the electronegativity, and alter adsorption tendencies by changes in adsorbate or adsorbent speciations. This section will analyze these areas of concern and attribute the potential threat to WTR adsorption in the context of the batch and column experiments in a cold weather region.

### 4.1.1 Surface Water Matrix

The adsorption solution utilized in the coagulation/flocculation process is surface water collected from the Red River of the North; located within two miles downstream of USGS gage: Red River of the North at Grand Forks North Dakota, site number: 05082500. Chosen water quality parameters is collected from "USGS Water-Quality Historical Instantaneous Data for the Nation", compiled and sorted within excel spreadsheets and organized to achieve descriptive statistics. For this study in particular, it is applicable to exploit river water as the coagulant solution because it's matrix is nearly congruent to the influent treated in the GFWTP. If these flocs were to be used as bioretention amendments in Grand Forks or towns nearby, they would exhibit the same floc characteristics applied in this experiment (assuming similar dosages and no polymers).

TABLE 4.1: Red River Matrix: Average concentration values and standard deviations from 2000-2017: USGA gage 05082500

| Parameter | Mean | St.Dev |
|---|---|---|
| Alkalinity, Filtered (mg/L)-$CaCO_3$ | 232.4 | 47.5 |
| Arsenic,filtered (ug/L) | 2.96 | 2.45 |
| Bicarbonate, filtered (mg/L) | 264.99 | 61.30 |
| Calcium, filtered (mg/L) | 66.50 | 12.95 |
| Chloride, filtered (mg/L) | 21.40 | 11.54 |
| Hardness (mg/L) - $CaCO_3$ | 324.36 | 76.73 |
| Iron, filtered (ug/L) | 23.34 | 55.13 |
| Magnesium, filtered (mg/L) | 38.74 | 11.31 |
| Nitrate + Nitrite, filtered (mg/L)-N | 0.70 | 0.56 |
| Orthophosphate, filtered (mg/L)-P | 0.12 | 0.055 |
| Orthophosphate, filtered (mg/L)-$PO_4^{3-}$ | 0.37 | 0.17 |
| pH,unfiltered,field | 8.08 | 0.34 |
| Phosphorus,unfiltered (mg/L)-P | 0.27 | 0.19 |
| Sodium, filtered (mg/L) | 41.92 | 25.25 |
| Sulfate, filtered (mg/L) | 170.98 | 74.96 |
| Suspended Solids, unfiltered (mg/L) | 174.98 | 182.89 |

Table 4.1 displays the mean values of pertinent matrix constituents and parameters

of the last 17 years at Grand Forks gage site mentioned above. Not all the constituents are listed, only the constituents and parameters possessing the potential to affect the adsorbate (P) or adsorbent (WTR). The major limitation to this matrix data, is that is disregards the seasonal matrix fluctuations. Parameters that have large standard deviations and confidence intervals will receive extra attention to ensure their presence is not excessive or absent in the time period of extraction. The remainder of this section addresses the potential adsorption ramifications of some of the crucial parameters listed in Table 4.1.

## 4.2 Matrix Parameters Potentially Inhibiting P Adsorption

### 4.2.1 pH

Many studies have determined adsorption behaves inversely with increasing pH. The affinity of DP for WTR materials partially depends upon the anions' complexing capacity, allowing binding to surface groups by ligand exchange reactions (inner-sphere complexes), and on the other hand, attractive or repulsive electrostatic interactions with the charged (hydr)oxide surfaces (Antelo, Avena, Fiol, Lopez, & Arce, 2005). Electrostatic interactions may be the limiting processes impacting P adsorption on WTR materials in the scope of this experiment. pH is a critical property that determines the phosphoric acid speciation as demonstrated in Figure 2.3, and indirectly influences the solution's zeta potential by altering surface group's charged surface. Regarding geolithe, Antelo and company point out at a sufficiently low pH the surface is mainly

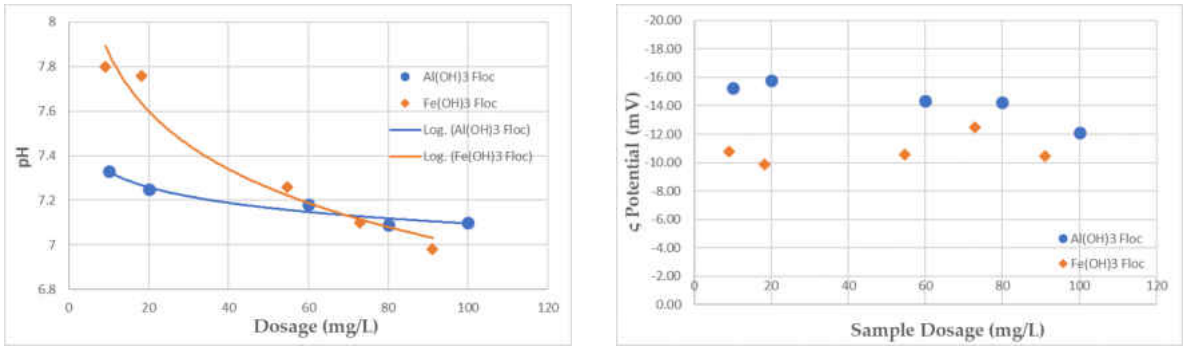


(A) (B)

FIGURE 4.1: pH and zeta potential plots. Diamond: $FeOH_3$ floc, circle: $AlOH_3$ floc (A): pH vs. coagulant dosage. (B): Zeta potential: data is not significant. Circle S= 0.718, diamond S= 1.022

populated with $FEOH_2^{1/2+}$ and $Fe_3OH^{1/2+}$ and at a high pH the surface is mainly populated with $FeOH^{1/2-}$ and $Fe_3O^{1/2-}$ (Antelo et al., 2005). These speciations will alter the zeta potential, affecting the P adsorption for outer-sphere complexation.

### 4.2.2 pH Effect on Zeta Potential

The zeta potential is the electric potential between the slipping plane of the double layer and the bulk fluid away from the interface. Zeta potential is a sound measure of the adhesion potential for the short, reversible reaction between the WTR amendments and DP because it quantifies the WTR floc outer-sphere complexation potential. A lesser absolute value of zeta potential means the negatively charged floc nucleus has a suppressed negative charge due to the the positively charged particles surrounding it (visually represented in Figure 2.5(A)). A lower pH naturally assists in helping destabilize solutions as positive charges are more abundant. Therefore, negatively charged DP are prone to greater adsorption potential as the WTR zeta potential is depressed.

Figure 4.1 contains plots demonstrating the relationship between coagulant dosages vs. pH and zeta potential. For outer-sphere adhesion, a smaller absolute value of zeta potential should be more conducive for adsorption of P on WTR. There is little to no change in zeta potential between the varying coagulant sample dosages, yet, there is a vivid parallel separation between $AlOH_3$ and $FeOH_3$ floc at their respective dosages. $FeOH_3$ floc exhibits less zeta potential values across the board, denoting a more destabilized solution, partially explaining why ferric chloride is the preferred (yet less popular) coagulant in waste water treatment. Interestingly, there is no viable change in zeta potential vs. amendment dosage. The only explanation to this conundrum is that the pH range does not vary enough to show a visible trend. Hypothetically, lets assume the pH varies 2-log (6-8) from an alum dosage of 0- 100 mg/L, Figure 4.2(A) demonstrates that in this pH range, the change in zeta potential is not explicit, which substantiates the data in Figure 4.1(B); however, for a larger pH range and pH values below 6, the change in zeta potential becomes more apparent.

Figure 4.2(B) exhibits the removal efficiency at varying pH and $PO_4^{3-}$ dosages. The removal efficiency does not alter significantly between a pH of 6.25 and 7.19; however, the efficiency drops approximately 10 percent between a pH of 7.19- 8.35. This aligns with previous studies indicating that the effectiveness of adsorbents notably decreases at higher a pH.

Based off the information presented in this section, pH has proven to have a profound influence of the WTR adsorption potential. It is profound in the sense that the change in pH may be a direct or indirect reason for altering adsorption potential of WTR. Lowering the pH ( optimally between 3-5) would completely destabilize a solution as the negatively charge particles become neutralized completely, consequently increasing the attraction forces between the $AlOH_3$ and $FeOH_3$ that surround the floc

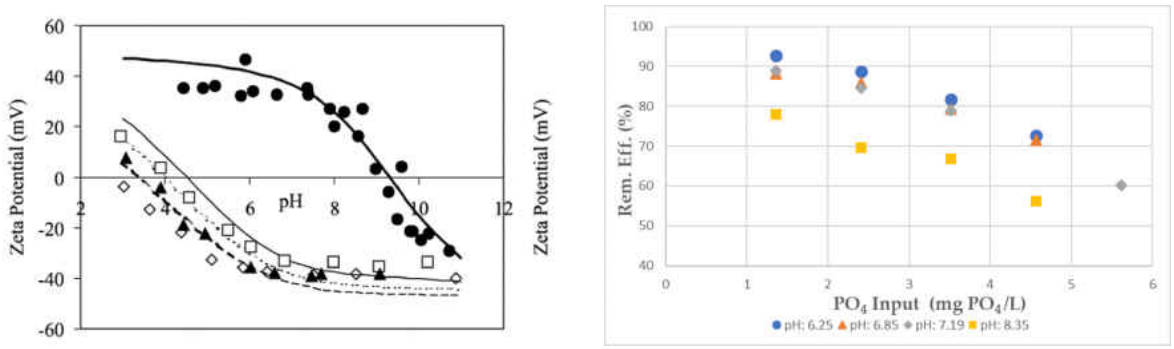


(A) (B)

FIGURE 4.2: Zeta potential and pH removal efficiency plots(A): Zeta potential vs. pH.(Antelo et al., 2005) (B): Removal efficiency vs. $PO_4$ inputs at varying pH

in the double layer. On the other hand, changing the pH also alters the speciation of the amendments and the solution substrates which may very well alter the electronegativity of particles (Figure B.1). Nevertheless more acidic solutions will possess a greater adsorption potential than basic solutions.

### 4.2.3 Calcium and Other Multivalent Ion Complexation

Antelo and associates also studied the repercussions of electrolyte occurrence in the adsorption process of P onto Geolithe (derivative of $FeOH_3$). They proved that the presence of electrolytes ($KNO_3$ and NaCl) depleted the adsorption of DP as they too competed for sorption sites. However, in the scope of this experiment, the ionic strength of surface water in cold weather regions do not exhibit waters with a high ionic strength so adsorption effects from monovalent cations are deemed nullified. Other prevalent divalent ions such as calcium and magnesium do have the capability to form complexes and precipitation products with DP however.

DP in solution may be immobilized via precipitation with multivalent metals such as aluminum, iron, calcium, and magnesium ions. Calcium phosphate can form compounds with DP as shown in Table 4.2. Calcium phosphate minerals are used in the production of fertilizers and are often responsible for nutrient loading of water bodies from surface runoff.

TABLE 4.2: Orthophosphate reactions with calcium ion

| Reaction | logK |
|---|---|
| Phosphate | |
| $Ca^{2+} + H_2PO_4^- \rightleftharpoons CaH_2PO_4^-$ | 1.408 |
| $Ca^{2+} + HPO_4^{2-} \rightleftharpoons CaHPO_4^0$ | 2.736 |
| $Ca^{2+} + PO_4^{3-} \rightleftharpoons CaPO_4^-$ | 6.459 |

As indicated in Table 4.2, calcium is present in the coagulation solution for the adsorption experiments ($C_{ave}$ = 66.50 mg/L) so it's reaction potential with DP must be addressed. The modes of adsorption and precipitation is dependent upon the loading of P in solution (Yagi & Fukushi, 2012). Studies have concluded that during low-medium loading of $PO_4$, adsorption is the only mode of removal of P from solution (0-50 $\mu$M/L), however at increased concentrations of $PO_4$, the slope of the isotherm deviates from the Langmuir isotherm suggesting there is another mode of $PO_4$ removal. $PO_4$ concentrations can possible be as high as 130 $\mu$M in surface water (Griffin & Jurinak, 1973).

To study the effect calcium has on the P adsorption in the scope of this project, an experiment was conducted to observe the difference in P removal based on varying calcium concentrations in solution. Calcium bicarbonate is added in increasing incremental dosages to the jars preceding the adsorption experiments. Next, the P solution is spiked to each of the four jars and then the residual P from solution is recorded. The

pH was held constant and the control contained the original solution matrix. The results are listed in Table 4.3 and verify that the concentration of calcium does not have an influence on the adsorption of P. Although, the equilibrium constants demonstrate calcium's complexation with DP, there is simply not enough time to at this small concentration range of P to permit these reactions from transpiring.

TABLE 4.3: $PO_4^{3-}$ concentration vs. calcium hardness concentration

| Sample | $PO_4^{3-}{}_{in}$ | $PO_4^{3-}{}_{out}$ | Ca. hardness - $CaCO_3$ |
|---|---|---|---|
| Control | 1 | 0.39 | 242 |
| 30 | 1 | 0.33 | 283 |
| 70 | 1 | 0.31 | 300 |
| 200 | 1 | 0.38 | 443 |

### 4.2.4 Effects of Turbidity

The effects of turbidity is speculated to have a negative effect on the adsorption of P on WTR. There is not a substantial amount of literature that support this claim, but the experiments conducted are performed at various NTUs, therefore this experiment will eliminate the turbidity variable altogether from the batch and column experiments.

Two experiments were conducted to observe the effects of turbidity on the adsorption of P. The first experiment consisted of two adsorption solutions. The first solution is a typical surface water coagulated solution that initially possessed about 54 NTU and after coagulation about 5 NTU. Second solution coagulated surface water but then artificial clay is added to the solution to increase the NTU back to 54 NTU; Therefore, the two solutions possess the same floc characteristics and solution matrix besides the turbidity level. $PO_4$ solution is spiked at intervals into the solutions and the residual P concentrations are recorded and converted to removal efficiencies. The results are illustrated in Figure 4.4.

The second experiment compared six different solutions coagulated with the exact same matrix but then artificial clay is added at increasing NTUs. P solution is spiked at a consistent interval four times and then the corresponding residual p concentrations are recorded. The results are depicted in Figure 4.3.

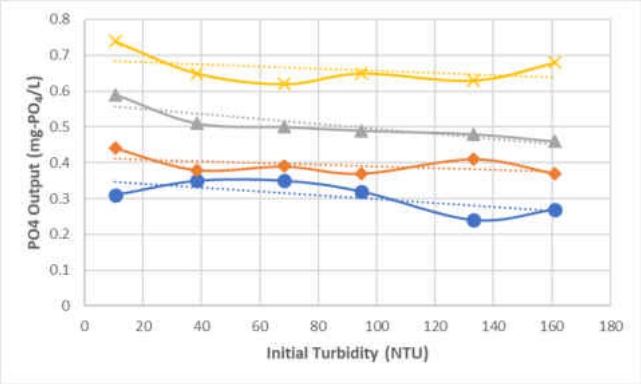


FIGURE 4.3: Turbidity experiment: residual $PO_4^{3-}$ output vs. turbidity. P Values: Circle (rd.1) : P=0.357, Diamond (rd.2) = 0.121, Triangle (rd.3) = .001, Cross (rd.4) =0.136

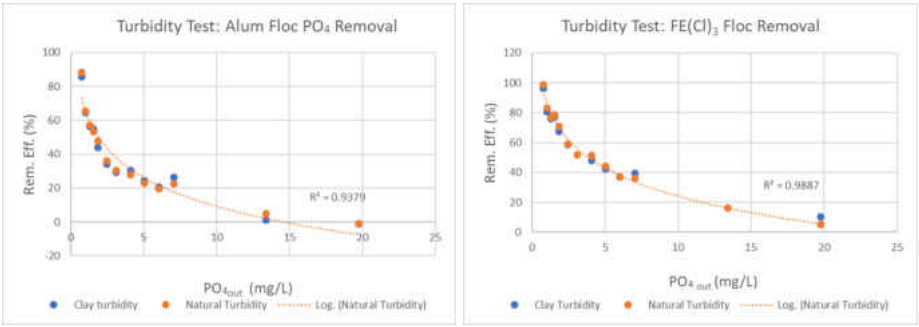


FIGURE 4.4: Turbidity experiment: removal efficiency plots for $FeOH_3$ floc and $AlOH_3$ floc

Figures 4.3 and 4.4 validates that turbidity in the scope of this experiment does not diminish P removal by WTR. Regarding Figure 4.3, linear trendlines are fitted to each round of spiked P at all six turbidity levels. The trendlines possess slight negative slopes but are not statistically significant (except Round 3) indicating that increased turbidity does decrease P removal from solution. This claim is further substantiated

by Figure 4.4. $FeOH_3$ and $AlOH_3$ floc at their respective turbidity levels both exhibited nearly identical removal efficiencies per P input dosage. In all, turbidity levels will not be taken into consideration during the batch and column adsorption experiments.

### 4.2.5 Chemical Precipitation of P in Water Treatment

The constituents and parameters aforementioned discuss how their presence possibly could inhibit the adsorption capacity of P on WTR. It is assumed when DP is introduced into solution, it adsorbs; however, chemical precipitation using alum and ferric chloride have been successful in wastewater treatment. Eq. 4.1 is an equation describing DP precipitation when alum is introduced to solution; conversely, Eq. 4.2 is the most applicable chemical equation when alum is introduced to solution in a typical surface water environment.

$$Al_2\,(SO_4) \cdot 14.3H_2O + 2PO_4^{3-} \rightleftharpoons 2ALPO_4 \downarrow + 3SO_4^{2-} + 14.3H_2O \tag{4.1}$$

$$AL_2\,(SO_4)_3 \cdot 14.3H_2O + 6HCO_3^{-} \rightleftharpoons 2Al\,(OH)_3 \downarrow + 3SO_4^{2-} + 6CO_2 + 14.3H_2O_3 \tag{4.2}$$

from Eq. 4.1, 1:1 is the molar ratio between Al to P which corresponds to a weight ratio 9.7:1.0, even greater dosages than this have been said to have been needed to precipitate P ( Hammer & Hammer, 2012). Naturally alkalinity is the competing specie in the precipitation process (Equation 4.2). As a result, in order to achieve 75 percent, 85

percent, and 95 percent, require alum to P weight ratios of 13 to 1, 16-1, and 22 to 1, respectively (Hammer & Hammer, 2012). Similar equations (Eq. 4.3 and Eq. 4.4) describe precipitation of DP or precipitation with hydroxide with the ferric ion in solution.

$$FeCl_3 \cdot 6H_2O + PO_4^{3-} \rightleftharpoons FePO_4 \downarrow + 3Cl^- + 6H_2O_3 \tag{4.3}$$

$$FeCl_3 \cdot 6H_2O + 3HCO_3^- \rightleftharpoons Fe\,(OH_3) \downarrow + 3CO_2 + 3Cl^- + 6H_2O \tag{4.4}$$

The mass ratio between DP and the metallic ion never reach a big enough ratio to achieve chemical precipitation. Secondly, the only P that is potentially precipitated is the initial P that exists in the river water when coagulation occurs. River water contains anywhere from 0.2–0.8mg/L–$PO_4^{3-}$. The removal efficiencies were very high nearly 100 percent removal, so the remaining spiked P to solution will be sorbed to the prexisting $FeOH_3$ floc or $AlOH_3$ floc. Table 4.4 shows some of the other chemical equations possible along with their corresponding equilibrium constants. As previously discussed with the calcium ion, chemical precipitation is not limited to the matrix but rather to the amount of time given for the reactions to transpire.

TABLE 4.4: Chemical equilibrium between phosphate and selected minerals at 25 °C

| Solid formed | Chemical equation | const. ($pK_a$) |
|---|---|---|
| Calcium hydrogen phosphate | $CaHPO_{4(s)} = Ca^{2+} + HPO_4^{2-}$ | 6.66 |
| Calcium dihydrogen phosphate | $Ca(H_2PO_4)_{2(s)} = Ca^{2+} + 2H_2PO_4^-$ | 1.14 |
| Hydroxyapatite | $Ca_5(PO_4)_3OH_{(s)} = 5Ca^{2+} + 3PO_4^{3-} + OH^-$ | 55.9 |
| Tricalcium phosphate | $Ca_3(PO_4)_{2(s)} = 3Ca^{2+} + 2PO_4^{3-}$ | 24.0 |
| Ferric phosphate | $FePO_{4(s)} = Fe^{3+} + PO_4^{3-}$ | 21.9 |
| Aluminum phosphate | $AlPO_{4(s)} = Al^{3+} + PO_4^{3-}$ | 21.0 |
| Magnesium ammonium phosphate | $MgNH_4PO_{4(s)} = Mg^{2+} + NH_4^+ + PO_4^{3-}$ | 12.6 |

## 4.3 Matrix Conclusion

After extensive research in pursuit of the potential impacts of the solution matrix, the primary parameter of concern is the pH. A higher pH will likely render better P removal performance because of its corresponding influence on speciation and zeta potential of the WTR. Other constituents and parameters such as divalent ions and turbidity are rendered inert as the contact time does not permit precipitation and other inhibitions from occurring. These are the sole parameters need to be accounted for in batch level experiments. The influence of NOM will be later addressed in the column results section to see if it's presence effects the WTR adsorption capacity. Now that the matrix has been addressed and validates that matrix parameters will not significantly influence P adsorption on WTR, the batch experiments can ensue.

# Chapter 5

# BATCH REACTOR ADSORPTION RESULTS

## 5.1 Introduction

This chapter exhibits the adsorption results and analysis of the batch adsorption experiments.The batch level experimentation is executed to strictly observe the adsorption characteristics of the adsorbate without the influence of other flow matrix parameters. Parameters such as hydraulic conductivity, media adsorption, contact times, etc. are neglected in these reactors so the adsorption characteristics can be understood before field level experimentation can eventuate. Adsorption will then be compared and contrasted to the column experiments to observe if the the adsorption characteristics resemble that in the batch reactors. Removal efficiency, residual P, and isotherms are the primary plots that are employed to illustrate the data and quantify adsorption or DP removal. The data is portrayed with excel plotting software but analyzed via Minitab18 to calculate statistical metrics that describe non-linear regressions that excel is incapable of performing. The log-normal charts used to describe the data and other referenced tables and figures in this section can be found in Appendix C and will not be included in the body of the chapter. The following section identifies the floc characteristics that influence its adsorption capacity in the batch reactors.

## 5.2 Batch Reactor WTR Amendment Characteristics

Amendments utilized as adsorbents include alum and ferric chloride coagulant flocs. These flocs constitute a conglomeration of the metallic (hydr)oxides derived from the coagulant in addition to the negatively charged colloids and suspended solids destabilized from solution. It is imperative to note that floc masses vary based on the turbidity of the solution. For instance, a surface water solution obtained in the winter may have a turbidity of 2.0 NTU, while surface water obtained during the spring may possess very high NTU. At an equivalent dosage of coagulant, the floc masses fluctuate even though the amount of coagulant does not. This is important because the quantitative adsorption isotherms measure the ratio of adsorbate (P) to adsorbent (WTR) and therefore, is highly sensitive to the inconsistent WTR mass. As proven in the previous chapter, turbidity levels do not influence P adsorption, adsorption is performed by the metallic (hydr)oxides that enveloping the bulk floc particles and not by the bulk mass itself. In order to quantitatively compare isotherms of different experiments, the isotherms will be normalized which is done by using the coagulant mass as the adsorption denominator instead of the floc mass. Albeit, it is the bulk mass that is utilized in the column and field experiments (not conducted in this experiment) to quantify adsorption capacity because the amount of coagulant cannot be discovered upon extraction (see Experimental Procedures and methodology chapter).

### 5.2.1 Saturated floc versus Dry floc

The majority of the batch adsorption and column experiments utilize amorphous (saturated) floc upon which it was conceived in the lab. This approach, although more difficult to measure, appears to be the more feasible method of implementation in

a bioretention cell rather than its aged (dried) counterpart; additionally, amorphous floc theoretically possesses a greater adsorption potential (Parfitt, Atkinson, & Smarat, 1975). Newly formed amorphous floc can become aged if dried or remains in solution for an extended period of time. Aging renders a crystalline structure essentially forming a less reactive arrangement of the adsorbent, limiting is binding energy and generating a more inert structure (Berkowitz, Anderson, & Amrhein, 2006). Contrarily, Table C.2 demonstrates that when dried floc is crushed into a fine powder, it actually performs better than its amorphous counterparts, contradicting the adsorption capacities indicated in Table C.1. Unfortunately, fine dried floc is susceptible to seeping through the media because it is smaller than the BMP media pores . Table C.2 additionally demonstrates that alum floc without the presence of a cationic polymer adsorbs more P than alum with a polymer, and the dried speciation adsorbed better for both dried and wet adsorbents. Aged floc have been known the exhibit different floc properties and are generally avoided to keep the experiment consistent. Despite the notion that the WTR amendments do all the adsorption of P, the supernatant must be taken into consideration.

### 5.2.2 Supernatant Adsorption

Theoretically, some metallic (hydr)oxides will not flocculate and associate with the floc particles, yet they may still yield adsorption along with other trace metals in solution; therefore, some adsorption may be performed by the supernatant. An experiment to observe the removal of DP by the supernatant revealed 5 percent removal out of solution, and the 60 mg/L sample removed 10 percent (Figure C.2). However, The data count is low and the confidence interval is very large, matter of fact, no P removal

is well within the 95% confidence interval (Figure C.2 (A)). Regardless, supernatant adsorption will be considered negligible in the experiments.

## 5.3 Normalized Isotherm Groundwork

Aforementioned, the floc mass is not a direct parameter that should be used to quantify adsorption; therefore, to relate adsorption performances between experiments, the isotherms will have to be normalized. The term normalized refers to relating adsorption quantities by comparing the added coagulant mass instead of the floc mass, floc mass depends on the turbidity, pH, and percentage of destabilization that transpires during coagulation and flocculation; although floc mass can be a fine indicator of adsorption, it does not properly quantify the adsorption performance because it is only the the coagulant (metallic (hydr)oxide) that adsorbs (in respect to the project parameters and constraints). So when referring to adsorption, instead of comparing the adsorbate mass per floc mass, the isotherm will be normalized and the adsorbate will be compared to the mass of metallic hydroxide yielded. Ideally, when the isotherms are normalized, the P adsorption should be equivalent at all dosages of coagulant. The removal of P however will likely be proportional to the coagulant dosage. A critical assumption is that the the floc product will solely complex with the hydroxide ion, a good assumption in water treatment at the pH range examined (Hammer & Hammer, 2012).

Table 5.1 are the metallic (hydr)oxide precipitate mass values used in normalizing the isotherms that correspond to the coagulant dosages in batch adsorption tests as derived from Eq. 4.2 & 4.4. Notice that the corresponding dosages of alum and ferric

TABLE 5.1: Mass of metallic (hydr)oxides per coagulant dosage

| Coagulant | Dosage (mg/L) | Mass (g) |
|---|---|---|
| Alum | 40 | 0.0104 |
| Alum | 60 | 0.0156 |
| Ferric Chloride | 36.4 | 0.0144 |
| Ferric Chloride | 54.6 | 0.0228 |

chloride are incongruent simply because in order to accomplish an equivalent mass of aluminum to ferric ions, a lesser concentration of ferric chloride renders equivalent mass to alum at a higher concentration dosage.

### 5.3.1 Normalization Effects on Adsorption

Figure 5.1 depicts the importance of normalizing isotherms in adsorption analysis. The experiment conducted in figure 5.1 compares the adsorption characteristics at varying initial turbidities to observe the corresponding adsorption effects. Both jars exhibit the same matrix and remove virtually the same mass of P depicted in Figure 5.1A, yet the isotherms diverge. This is a perfect example of why using the floc mass as the adsorbent diverges from the true adsorption nature of the amendment. Once both isotherms have been normalized (Figure 5.2) the isotherms portray identical adsorption capacities indicating no significant statistical difference (P= 0.00); namely, the adsorption per $C_{eq}$ is not discrete.

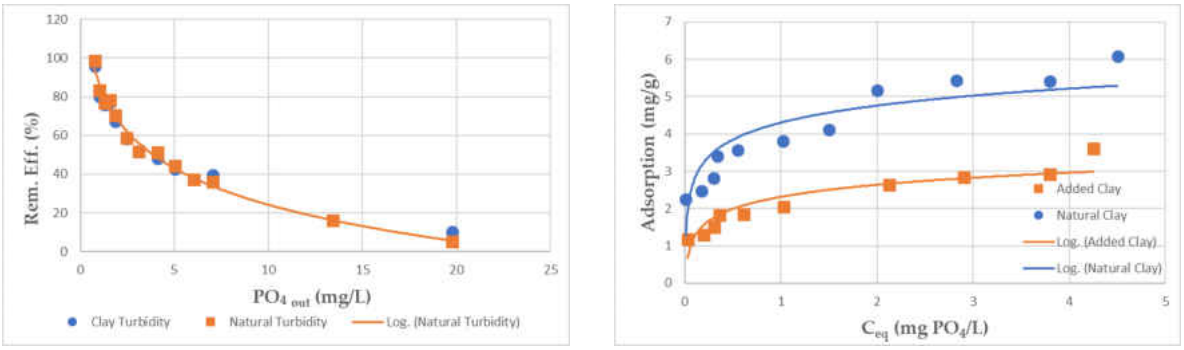


(A) (B)

FIGURE 5.1: 54.6 mg/L $FeCl_3$ removal efficiency and adsorption plots (A): Removal efficiency plot (B): Adsorption isotherm: Artificial clay S=0.340. Natural Clay: S=0.509

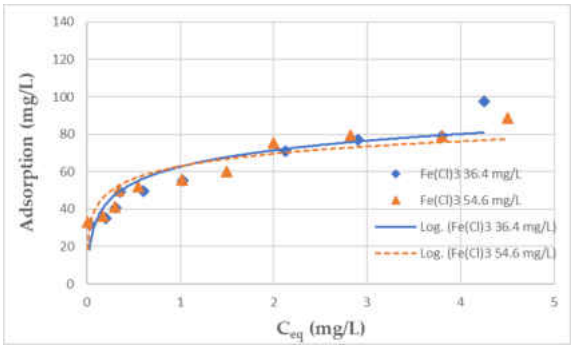


FIGURE 5.2: Normalized isotherms of Figure 5.1B. Artificial clay: $R^2$= 0.839, S= 9.196. Natural Clay: $R^2$= 0.793, S= 9.170.

## 5.4 Normalized Isotherm Results

In theory, normalized isotherms for the same adsorbent, should exhibit the same normalized adsorption quantities across experiments (assuming similar pH and temperatures). Although this theory holds true between the majority of isotherms of the same experiment, it does not harvest congruent results across batch reactor experiments. Figure 5.3 and 5.4 is one of the many normalized isotherms that demonstrate the impact of normalizing isotherms. More normalized isotherms are located in Appendix C.

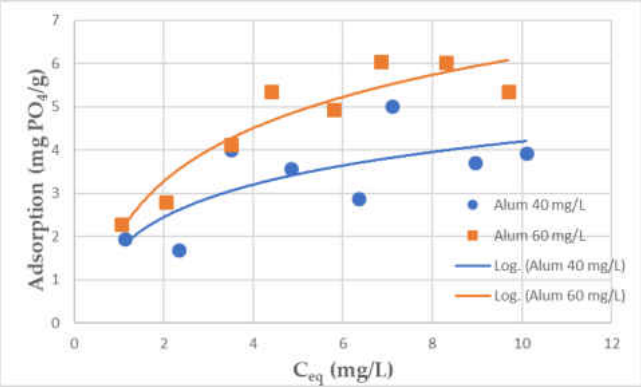


FIGURE 5.3: Batch reactor adsorption plot: 3-22 $AlOH_3$ floc non-normalized isotherms

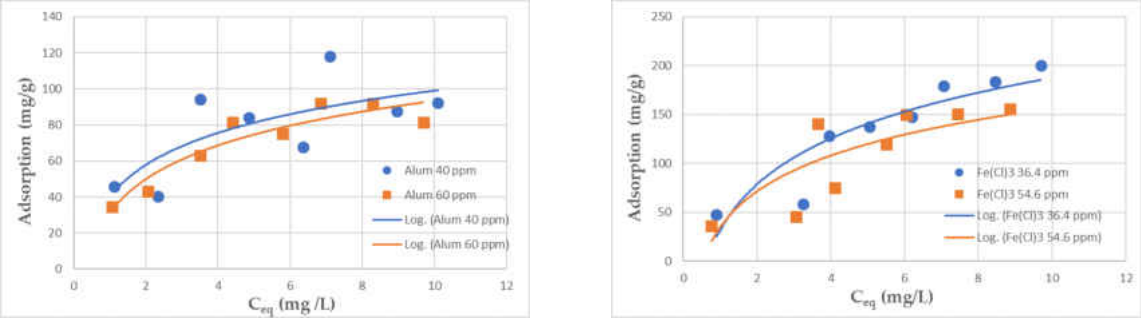


(A) (B)

FIGURE 5.4: Batch adsorption experiment (3-22) (A): Normalized isotherms ($AlOH_3$ floc) (A): 40 mg/L : $R^2$= 0.529, S= 19.354. 60 mg/L: $R^2$= 87.9, s= 8.125. (B): Normalized isotherms ($FeOH_3$ floc) 36.4 mg/L: S= 25.575 $R^2$= 82.4. 54.6 mg/L: s=30.908 $R^2$= 66.8

### 5.4.1 Batch Reactor Removal Efficiency

Many studies acknowledge removal efficiency is not a great metric in describing batch adsorption studies because it is a function of the amount of amendment and does not necessarily describe the inherent adsorption potential; nonetheless, it does illustrate the variation in P removal effectiveness between $AlOH_3$ floc and $FeOH_3$ floc at equivalent dosages. Figure 5.5 illustrates the logarithmic relationship between the P input and removal efficiency. The $AlOH_3$ and $FeOH_3$ removal characteristics mirror each

other indicating similar characteristics yet $FeOH_3$ appears to be more robust. When the plots are combined (Figure 5.6), $FeOH_3$ floc clearly out performs $AlOH_3$ floc approximately 20 percent more effectively per all equivalent P inputs. Figure C.8 in Appendix C shows the log-normal plots with confidence intervals. Next, the removal efficiency metric will be compared with the adsorption capacity results to determine the relationship that exists between the two.

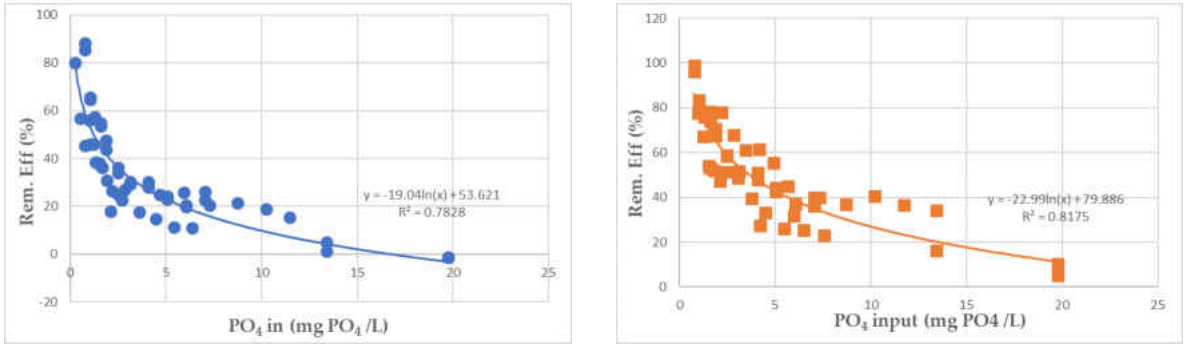


(A) (B)

FIGURE 5.5: Composite removal efficiency plots (A): Alum 60 mg/L floc P removal. s= 9.74, $R^2$= 0.783, P= 0.000 (B): $FeCl_3$ 54.6 mg/L floc removal. s= 9.248, $R^2$= 81.79, P= 0.000

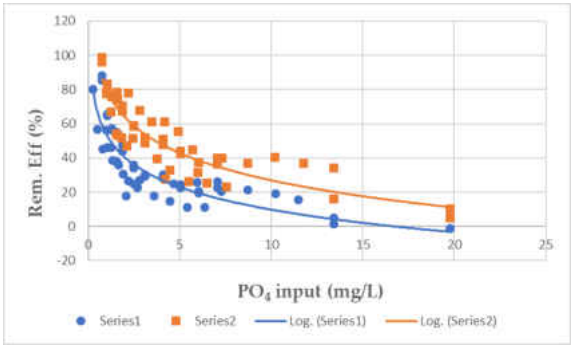


FIGURE 5.6: Aggregate batch reactor removal efficiency data for $AlOH_3$ and $FeOH_3$

## 5.5 Batch Reactor Non-normalized Isotherm Results

The normalization technique received a lot of attention and praise in the previous subsections, however upon experimentation, there exists strong adsorption relationships amongst experiments without normalizing the ordinates across experiments. Figure 5.7 depicts the aggregate adsorption capacities at of all the experimental adsorption ordinates at their respective $C_{eq}$. $FeOH_3$ floc evidently, increasingly diverges from it's $AlOH_3$ counterpart at their respective $C_{eq}$ for the given range. This is supported by Figure 5.6 in which the $FeOH_3$ floc outperformed $AlOH_3$ flocs removal efficiency. Albeit, the isotherms do not depict the adsorption by the metallic hydr(oxide) the aggregated data appeared to eclipse the normalization caveat. This is likely because the turbidity between experiments did not vary substantially and alter the adsorption trends, which does not dismiss the fact that the adsorption values are undermined by the floc mass but is minimized in the experimental settings. Individual plots with confidence interviews may be reviewed in Figure C.4.

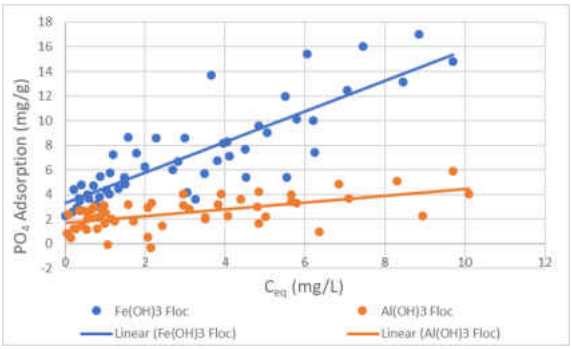


FIGURE 5.7: Aggregate non-normalized isotherm comparison (A): $AlOH_3$ floc: $R^2$= 34.81, S= 2.194, P=0.00. $FeOH_3$ floc: $R^2$= 71.62, S= 2.03, P= 0.00

## 5.6 Batch Reactor Adsorption Recap

The batch reactor experiment results clearly demonstrate that $FeOH_3$ floc is the superior WTR amendment as both the aggregate removal efficiency and non-normalized isotherm plots clearly distinguish a performance gap between the WTR amendments. This was fist speculated in section 4.2.1 above when the absolute value of the $AlOH_3$ floc consistently possessed a greater value than $FeOH_3$ floc indicating a greater positive charge in the double layer enhancing the attraction for negatively charged substrates. $AlOH_3$ adsorption appeared to become exhausted near 4 $mg/g$ were $FeOH_3$ adsorption capacity is still increasing even at a $C_{eq}$ greater than 10 $mg-PO_4/L$. Normalizing isotherms did not gain the analytical credibility as first assured in the beginning of this chapter, as the non-normalized adsorption isotherms rendered more realistic data across varying batch reactor experiments. These adsorption capacities will be compared with the column experiment data and literature review capacities in the discussion chapter to see how the adsorption of WTR compared to similar amendments.

# Chapter 6

# COLUMN EXPERIMENT RESULTS

## 6.1 Introduction

The batch reactor test solely observes the WTR amendment adsorption characteristics in the absence of influential variables that exist in the field. The column test employs other pertinent variables that may affect adsorption capacities. These variables are imperative because they better describe the the adsorption characteristics of a bioretention cell or sand filter BMP. One parameter of interest is the adsorption kinetics. From the kinetics experiment (mentioned in 1.3.2), full adsorption proceeded in minutes in a batch reactor. Contact times in one literary study observed 300 seconds between the sand amended media and 1.73-2.42 seconds with the amendment particles, indicating that there are only a few seconds for adsorption to transpire (Erickson et al. 2012). Luckily, the outer-sphere complexation is very liable so adsorption should occur quickly. The hydraulic loading of the column experiments ranged from 8-11 mL/ min; although rather rapid, the amended columns adsorb a substantial fraction of what is observed in the batch reactor experiments. This chapter presents the data collected from the column experiments and generalizes the results. Further statistical analysis will be demonstrated in the discussion chapter. Log- normal plots, figures, and some tables mentioned but not incorporated in the chapter, are placed in Appendix D.

### 6.1.1 Analysis Technique

The primary objective of the column experiment is to discover peak adsorption capacity, P retention upon desorption, and removal capabilities of the amended column. At peak adsorption, the column ceases to adsorb P and will release P greater than $P_{in}$ into the effluent. The column is said to be at it exhaustion depth (ED) once the peak adsorption has occurred. The ED parameter is a normalized value because it is independent of the column surface area and will allow the engineer to discover the design P loading before the BMP media should be replaced with fresh amendments. Along with the ED, other metrics like adsorption capacity and removal efficiency will help describe the column performance in the adsorption, desorption, and multi-cycle plots. Unlike the batch adsorption study, the adsorption plots cannot be normalized because there is no way in quantifying the coagulant mass. This is because the flocs employed in the column is extracted from the jar tests collectively, which cannot directly measure the metallic (hydr)oxide mass. Table 6.1 is the complete list of all the column experiment and their parameters.

TABLE 6.1: Column experiment parameter summary

| Trial | Floc | Mass (g) | Loading (ml/min) | solution | pH | $PO_4$in.(mg/L) |
|---|---|---|---|---|---|---|
| A | $ALOH_3$ | 0.2060 | 7.4 | Distilled | 5.8 | 1.89 |
| B | $ALOH_3$ | 0.2031 | 9.0 | Distilled | 5.8 | 1.95 |
| C | $FEOH_2$ | 0.6512 | 8.0 | Distilled | 5.8 | 1.98 |
| D | $AlOH_3$ | 0.1514 | 10.0 | Surface Water | 7.9 | 1.97 |
| E | $FeOH_2$ | 0.4793 | 10.0 | Surface Water | 7.9 | 2.00 |
| F | $FeOH_2$ | 0.2758 | 10.0 | Surface Water | 7.9 | 2.00 |
| G | $AlOH_3$ | 0.4105 | 11.0 | Surface Water | 7.9 | 2.02 |
| I | $AlOH_3$ | 0.1477 | 9.0 | Surface Water | 7.6 | 2.00 |
| J | $AlOH_3$ | 0.2577 | 8.5 | Surface Water | 7.9 | 1.86 |

Input P concentration varies from experiment to experiment but should render negligible because the variance is minuscule, likewise for the hydraulic loading. The column experiments implement $AlOH_3$ and $FeOH_3$ floc that primary use floc mass as the dependent variable. The pH of solution will likely dictate the sorption capacity for P removal as well. The column experiments can be described by single adsorption cycles, desorption cycles, and multi-cycle analysis. Single adsorption experiments describe a single event P capture capacity for the column, which usually initiates with the maximum sorpion potential. The desorption and multi-cycle experiments help describe the longevity of the column P retention and the percent of P that is retained from cycle to cycle. Spearman Rho correlation matrices comparing adsorption and P capacity parameters are utilized in determining relevant relationships among the column parameters.

## 6.2 Phosphorus Fate in Column: Cycle 1

### 6.2.1 Breakthrough Curve

Before assuming the WTR will be the sole adsorbent, a break through curve (control) will indicate how much P the column can remove in the absence of amendments and depicts the column response time before sensing the influent P solution. Figure 6.1 is the breakthrough curve demonstrating the media is completely inert and takes nearly 10 minutes for the solution to be entirely immersed in the column; however, 10 minutes is the maximum breakthrough estimation because the P value is taken as an average of a four minute extraction interval, so the actual breakthrough could be even sooner. Overall it is safe to assert that the column media contributes to zero P adsorption.

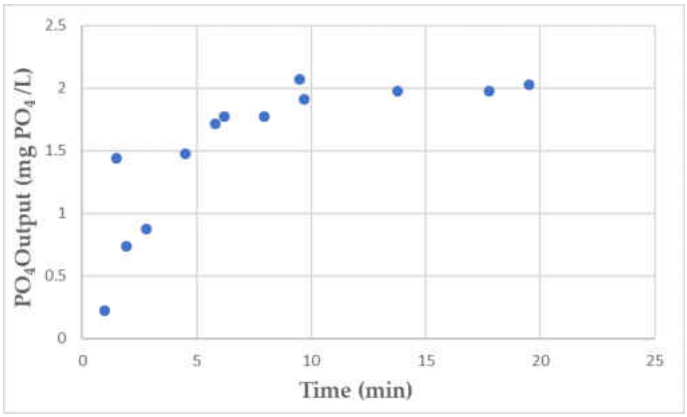


FIGURE 6.1: Column breakthrough curve (Ottawa sand). Hydraulic loading: 8.0 mL/min

### 6.2.2 Cycle 1: Analysis Limitations

Many of the single cycle experiments perform the adsorption characteristics of one adsorption/ desorption cycle. The column at this phase has the maximum potential to adsorb P because it possesses very little occupied sorption sites. Observing this cycle exclusively would be naive because in reality, the BMP is exposed to multiple rounds of runoff events. In a single cycle, $C_{eq}$ equals the effluent P concentration ($C_{eff}$), this cannot be assumed for following cycles as the P concentration in the column will be different than the $C_{in}$ and $C_{out}$; namely, $C_{eff} \neq C_{eq}$. Another experimental parameter disregarded is the dry antecedent period. During this period, amendments and other media are subjected to crystallization which may render the amendments inert and potentially less effective, subsequently, the influent that remains in the column for an extensive period of time can be subjected to slow irreversible inner-sphere complexation with the amendments. Figure 6.2 depicts the residual P response versus TD that portray the effects of stagnant solution within the column. Figure 6.2(A) delineates the raw data over that course of a three day adsorption experiment. The experiment was discontinued and resumed twice.

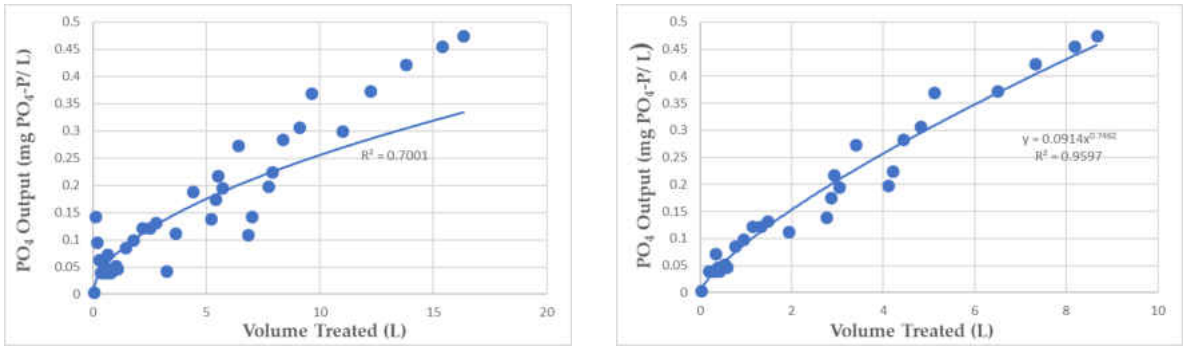


(A) (B)

FIGURE 6.2: Cycle 1: antecedent period effects with 0.6521 g. $FeOH_3$ floc
(A): Raw data (B): Raw data, no outliers

Aforementioned, for short contact periods the primary adsorption mechanism is by outer-sphere complexation; however, the adsorbent retained in the column for the extended period of time is subjected to the slow irreversible inner-sphere complexation, and ion exchange (see Figure 2.5). These mechanisms enhance the adsorption as indicated in Figure 6.1(A). Figure 6.1(A) contains two dips in P residual output, both dips occur at the beginning of the previous days experiment. Although this adsorption mechanism is a more permanent removal method, it is not a mechanism that describes the P removal performance a single cycle adsorption experiment. It does however depict the adsorption mechanisms that occur during the antecedent period of a multi-cycle analysis. Figure 6.2 is a prime example of the effects of experimental stoppage mid experiment, and substantiates the assumption of eliminating outliers from the data to better represent the true data set. The outliers due to the experiment discontinuation are erased in Figure 6.1(B) and improved the functions $R^2$ from 0.7001 to 0.9597. Outliers due these environmental factors will not be remain in the data sets to be analyzed unless chosen to be analyzed on an event basis.

### 6.2.3 Potential NOM Adsorption Effects

Filtered surface water is the column influent solution employed in more than half of the column studies as indicated in Table 6.1. Using this solution renders a more realistic performance curve of a similar stormwater matrix that would be applied to a cold region bioretention BMP. A primary adsorbate that is proposed to compete with P for adsorption sites is NOM. A column experiment utilizing a surface water matrix, collected the residual P values along with the adsorbate readings using a UV spectrophotometer at 254 nm. This absorption reading is compared with the the breakthrough curve as depicted in Figure 6.3 which demonstrates that NOM is almost entirely inert through the column. NOM must require ligand attachment and inner-sphere complexation to be absorbed by the amendments, this is not surprising however as the effects of calcium and other other constituents also proved to be inert. See figure D.1 for curve with confidence intervals.

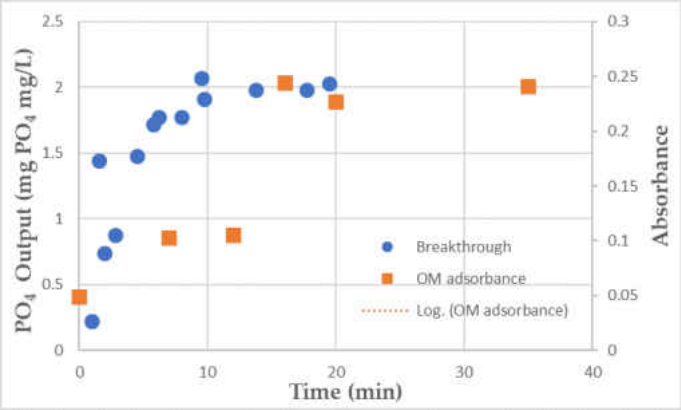


FIGURE 6.3: NOM residual plot. Circle= Breakthrough points, Square= OM absorption points. P= 0.004

### 6.2.4 Adsorption Cycle 2 Comparison

If adsorption through the column is successful, P will remain in the column ensuing a rinse (desorption cycle). Depending on the percent desorption, the second adsorption cycle is likely to be less effective than the previous due to limited available sorption sites.

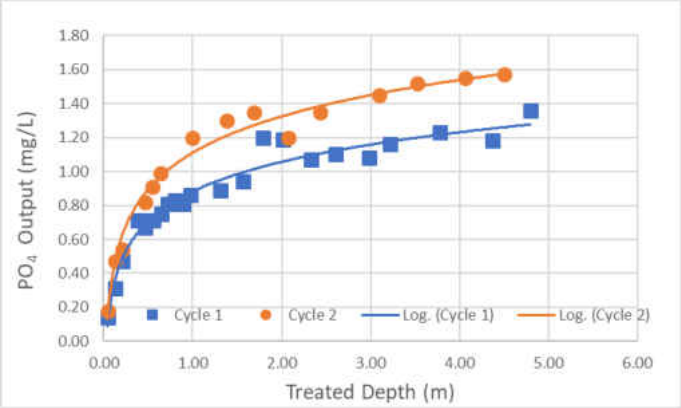


FIGURE 6.4: 0.2031 g $AlOH_3$ residual P plot comparing the first and second adsorption cycles. Cycle 1: S= .0218, $R^2$= 0.978. Cycle 2: S= 0.0219, $R^2$= 0.956

In this particular experiment, the column retained 67.78 percent of the influent P load upon first cycle and retained 45.91 percent of the total P loading on the second.Theoretically, the plot ordinates will continue to increase until the column has reached $C_{eq}$ were the regression line will be completely vertical as the column has no sorption sites remaining. Similar results across experiments are achieved and will be further substantiated in the discussion section.

## 6.3 Cycle 1: Cumulative Mass Retained

A quality metric to quantify and compare the effectiveness of P adsorption is by comparing the total mass influent and total mass retained in the column. The mass of P retained is discovered simply taking the definite integral of the regression equation of the residual P vs. volume treated plot. sequentially, the difference between the P influent and the integration value obtains the mass P retained in column at any response location. This value is presented by Equation 3.4.

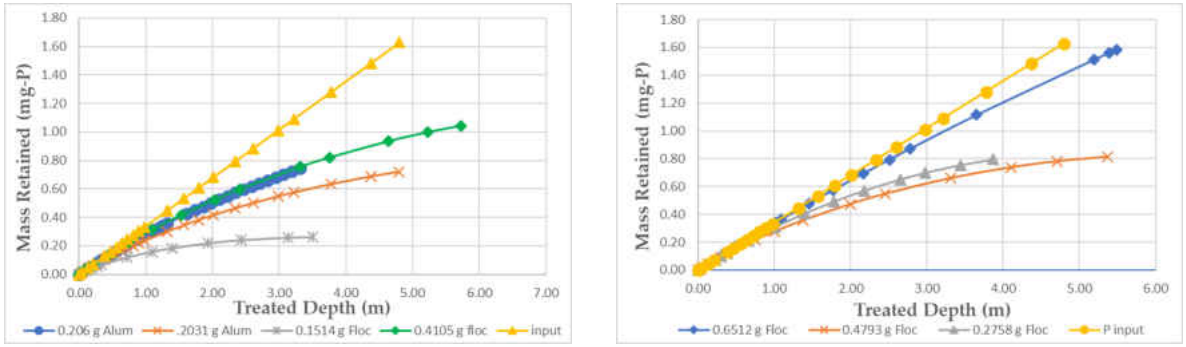


(A) (B)

FIGURE 6.5: Empirical cumulative mass retained in columns (A): $AlOH_3$ floc (B): $FeOH_3$ floc

TABLE 6.2: Empirical mass retained values

| Vol | TD | A | E | F | J | I | B | D | C | G |
|---|---|---|---|---|---|---|---|---|---|---|
| 0.5 | 0.94 | 0.267 | 0.260 | 0.289 | 0.165 | 0.186 | 0.199 | 0.143 | 0.311 | 0.274 |
| 1 | 1.88 | 0.482 | 0.453 | 0.512 | 0.238 | 0.278 | 0.312 | 0.216 | 0.601 | 0.493 |
| 1.5 | 2.83 | 0.663 | 0.600 | 0.676 | 0.276 | 0.335 | 0.371 | 0.252 | 0.874 | 0.673 |
| 2 | 3.77 | 0.815 | 0.707 | 0.785 | 0.292 | 0.369 | 0.389 | 0.261 | 1.131 | 0.821 |

Letters correspond to experiments located in Table 6.1.

Figure 6.6 demonstrates the empirical P retained vs. the mass of adsorbent per volume treated. Both regression lines indicate strong relationships with increasing P retention per WTR amount. There could be other parameters that are possibly driving

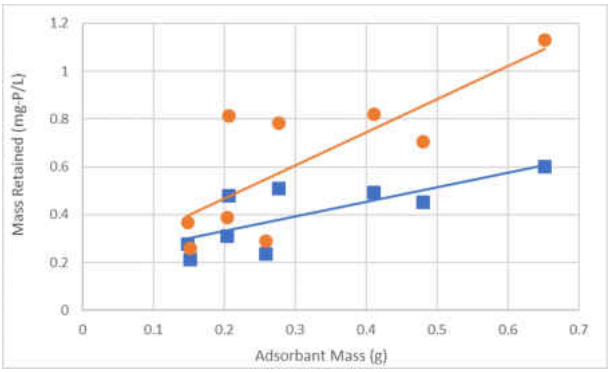


FIGURE 6.6: Empirical P retained vs. mass of adsorbant at a given volume treated. 1 L (Circle): $R^2$= 0.717, P= 0.03. 2 L (Square): $R^2$= 0.733, P= 0.025

P retention as well. Table D.1 and D.2 show the Spearman Rho correlation matrix between the adsorbate mass retained, hydraulic loading (rate), pH, and input P. Both tables statistically confirm that there indeed is a correlation between the mass of adsorbate and mass of adsorbent. There also exists relationships between The rate and pH and P input, but are likely to be coincidental and complimentary, for instance, the P intake is directly proportional to the the rate of influent. Figure 6.5 provides and excellent visualization of the adsorption dissipation throughout the progression of the event. Perfect retention occurs when the slope is equal to the input line (linear line). When the slope diverges from the input, the column does not adsorbs a fraction of the input P. Once the plot completely levels off like it does for 0.1514 sample, the adsorption sites are saturated and cannot remove influent P. The next chapter will expound the potential for adsorption by means of single adsorption cycle and discover the ED and maximum adsorption potential.Next section analyses the desorption capabilities of the amended columns.

## 6.4 Column Desorption Results

### 6.4.1 Introduction

An imperative property in the realm of BMP performance is the ability for the amended column to retain the P it adsorbs. If the adsorption process can be reversed, the adsorption is offset and rendered ineffective. Leaching (desorption) is a common event amidst bioretention and occurs even during dry periods ensuing an event. Leaching is susceptible for loosely attached adsorbate also know by their reversible reactions. This leaching is relevant in the scope of this experiment because the short contact times and outer-sphere complexation, which leaves the column susceptible. This section quantifies the amount of P desorbed from four column tests and characterizes the general desorption tendencies.

### 6.4.2 Desorption Results

Figure 6.7 demonstrates the aggregation of two two cycle column experiments, both columns contain $AlOH_3$ floc at their respective masses. The plots illustrate the desorption from the first and second cycle are virtually identical, namely, the desorption rate does not change upon cycles. The plot also illustrates that there is a discrepancy between the amount of P desorbed; however, if assumed that the cycles do not change P desorption, Figure 6.7(B) demonstrates there is a strong correlation between all desorption cycles.

Table 6.3 tabulates the percent desorbed using a derivation of the regression line equation in Figure 6.7(B). Initially nearly 50 percent of P input is desorbed, but the

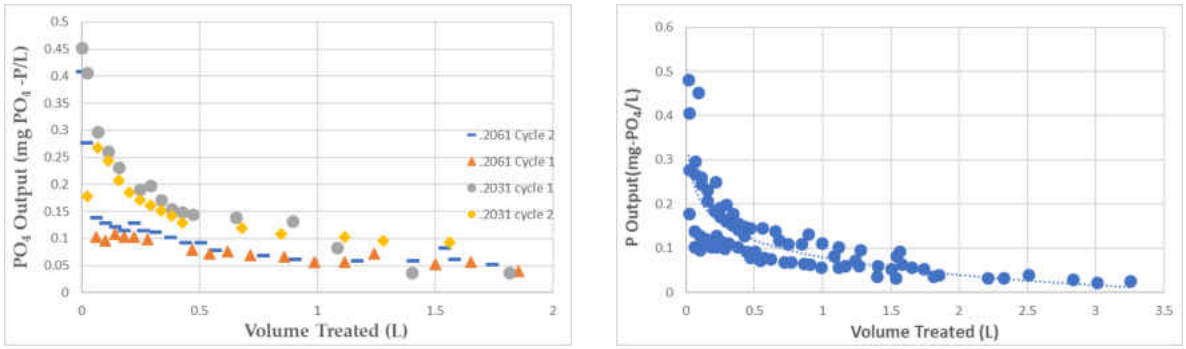


(A) (B)

FIGURE 6.7: Aggregate desorption (A): P residual charts comparing the first and second desorption cycles. Triangle: S=.00912, $R^2$= 89.5.Dash: S=.0215, $R^2$= 0.827. Circle: S= 0.01427, $R^2$= 98.1. diamond: S= 0.0312, $R^2$= 68.0 (B): Aggregate residual P plot. $R^2$= 0.6206, S= 0.0577 P=0.000

TABLE 6.3: Percent desorbed at given volume treated

| Vol (L) | Rem eff (%) |
|---|---|
| 0.02 | 46.67 |
| 0.10 | 31.86 |
| 0.20 | 25.76 |
| 0.29 | 22.59 |
| 0.43 | 19.31 |
| 0.50 | 17.89 |
| 0.62 | 16.10 |
| 0.72 | 14.85 |
| 0.85 | 13.41 |

rate quickly curtails and likely only desorbs 10 percent after 1 L of treated volume. The log- normal scatter plot containing confidence intervals may be viewed in Figure D.2 in Appendix D. Desorption analysis will be particularly useful in the upcoming multi-cycle analysis.

## 6.5 Multi Cycle: Adsorption Analysis

### 6.5.1 Introduction

The cyclical nature between events is also of interest in the realm of bioretention performance. Unlike the previous single cycle experiments, each subsequent cycle possesses less sorption capacity, decreasing the columns effectiveness. Analysis of a multi-cycle experiment differs from single cycle analysis because $C_{eff}$ also does not equal $C_{eq}$ which is the independent variable used in the single adsorption cycle isotherms. This is because the residual P value exiting the column does not represent $C_{eq}$ due to the preexisting concentration from the preceding event; therefore, isotherms for the multi-cycle results will not be employed and replaced by cumulative P retention to describe the performance analysis.

### 6.5.2 Cumulative P Retention Analysis

To calculate cumulative P retention in column, observed values will be represented by the integration of the goodness to fit regression equations derived from the residual P plots. An accurate regression line is imperative because the calculation for P retention is only as reliable as the regression upon which the data is integrated. Figure 6.8 illustrates the goodness to fit regression line overlaying the raw data for the 0.2031 g $AlOH_3$ floc double cycle experiment. It is evident that the goodness to fit regression line does an excellent job delineating the raw data. This also remains true when analyzing the other three mulit-cycle residual P plots indicating that the empirical calculations for the cumulative P retention in columns is reliable.

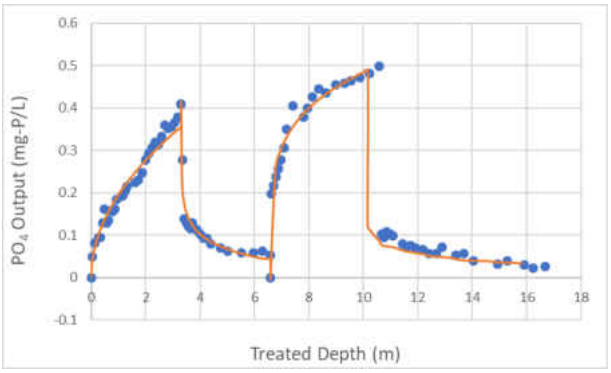


FIGURE 6.8: 0.2031 g alum floc regression line delineation of residual P raw data.

the Figure 6.9 exhibits the hysteresis of the P output between a routine three cycle event. Subsequent cycles visually contain less capacity for adsorption and desorption, appearing to equalize at 0.15 mg-P. This equilibrium P value demonstrates the permanent P that will retain in column indefinitely. The loosely bound P is desorbed with each desorption cycle and will continue to desorb until all available sorption sites are occupied with semi-permanent strong bonds.

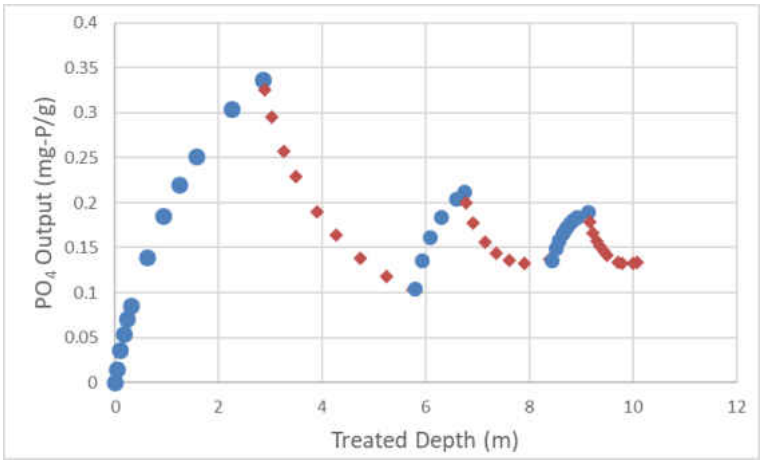


FIGURE 6.9: Triple cycle P retention amended with 0.1477 $AlOH_3$ floc. Circle= adsorption, Triangle= desorption.

Figure 6.10, 6.11, 6.12 exhibit the remaining residual P adsorption cycles with their

corresponding empirical cumulative mass retained plots. Figures 6.10(B) and 6.12(B) both have general increasing mass retainment trends but Figure 6.11 (B) does not. This is because the previous cycles in the progression did not reach its maximum adsorption potential upon completion (the experiment was cut short). If the cycles were prolonged,they undoubtedly would look like Figure 6.11(B) except with a higher equilibrium mass.

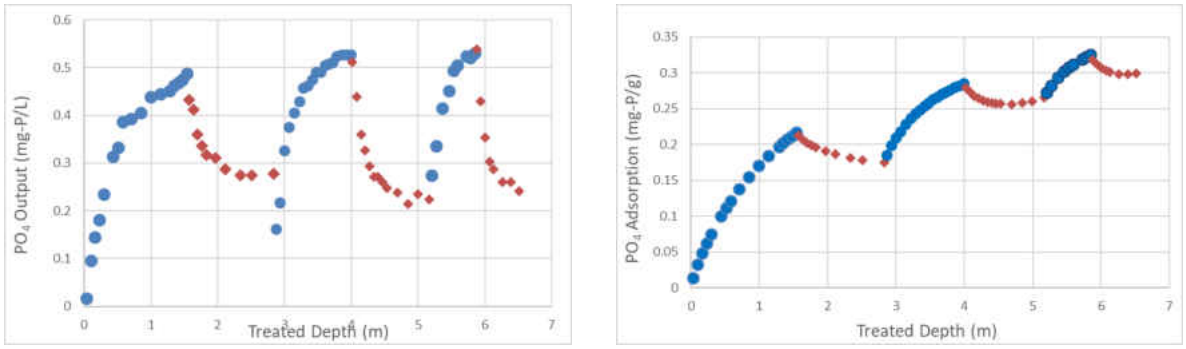


(A) (B)

FIGURE 6.10: 0.2577 g $AlOH_3$ data. Circle= adsorption, triangle= desorption (A): Raw residual P data (B): Cumulative mass retained plot

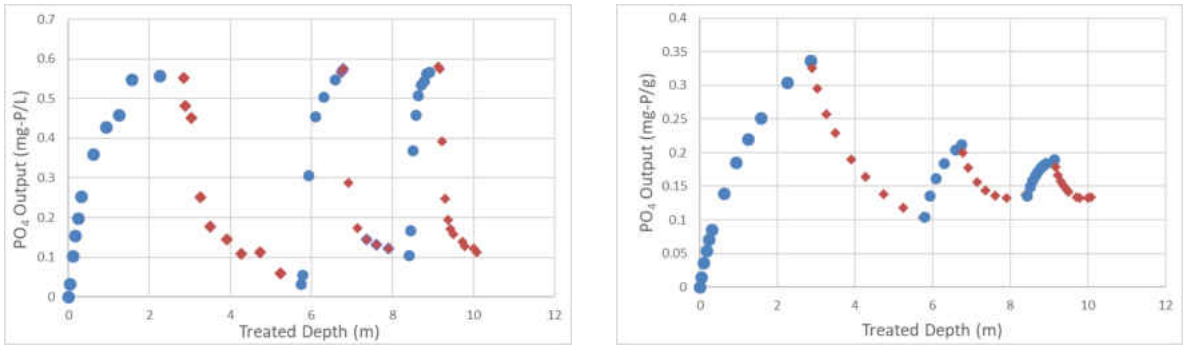


(A) (B)

FIGURE 6.11: 0.1477 g $AlOH_3$ data. Circle= adsorption, Triangle= desorption (A): raw residual P data (B): cumulative mass retained plot

As mentioned previously, the adsorption/desorption capacity decreases after subsequent cycles; Figure 6.13(B) is a prime example of this adsorption capacity reduction. When the adsorption cumulative mass plot designates a zero slope, the column

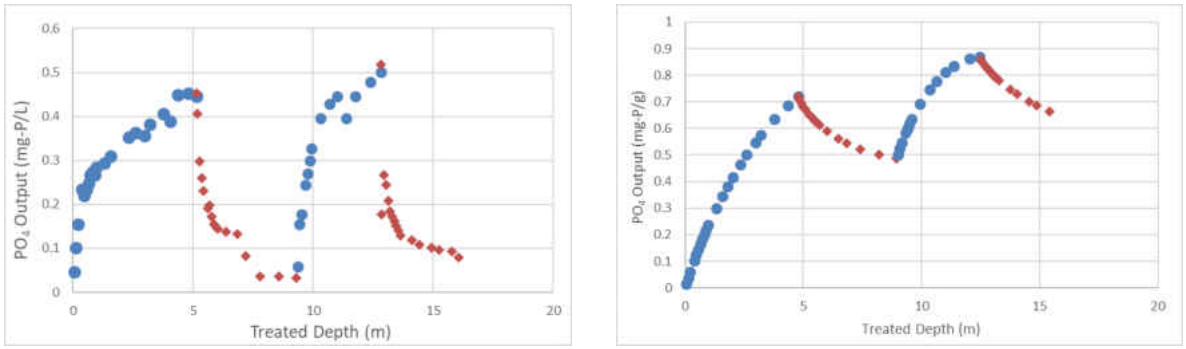


(A) (B)

FIGURE 6.12: 0.2031 g $AlOH_3$ data. Circle= adsorption, Triangle= desorption (A): raw residual P data (B): Cumulative mass retained plot

has reached equilibrium and will retain a constant P mass, contributing no P removal from the influent for upcoming events. Despite a vivid decrease in adsorption between event cycles, the desorption characteristics remain consistent between cycles. Figure 6.14 is another triple cycle experiment were the adsorption reduction looks similar to that of Figure 6.13(B) but the desorption does not appear to change between cycles (Figure 6.14(B)). So while the adsorption capacity decreases from cycle to cycle, the desorption rate remains fairly constant. Referring too the cumulative mass retained plots, the adsorption magnitude distinctly reduces between cycles while the desorption magnitude is more obscure, namely, there is less indications of changes in the desorption characteristics between cycles. These observations are consistent with the desorption analysis in Chapter 6.4 were the desorption characteristics are relatively congruent between cycles and events.

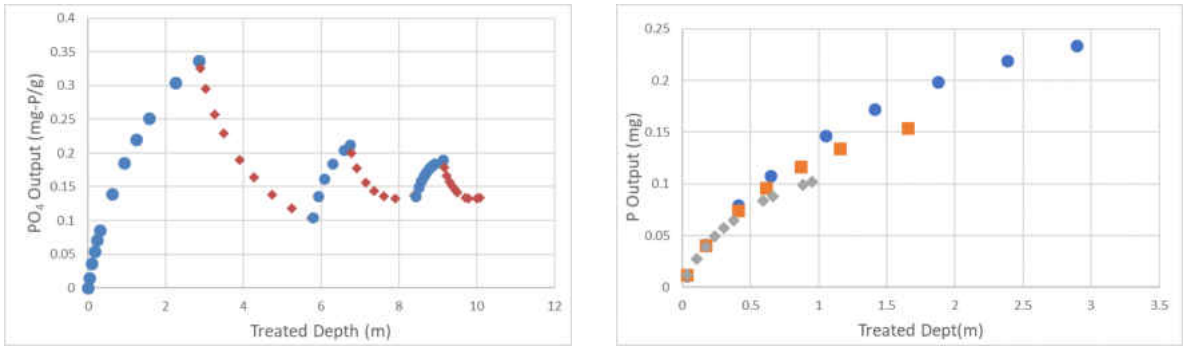


(A) (B)

FIGURE 6.13: (A): Cumulative mass retained (B): Adsorption cycles: cumulative mass retained. Circle = cycle 1, Square= cycle 2, Diamond= cycle 3.

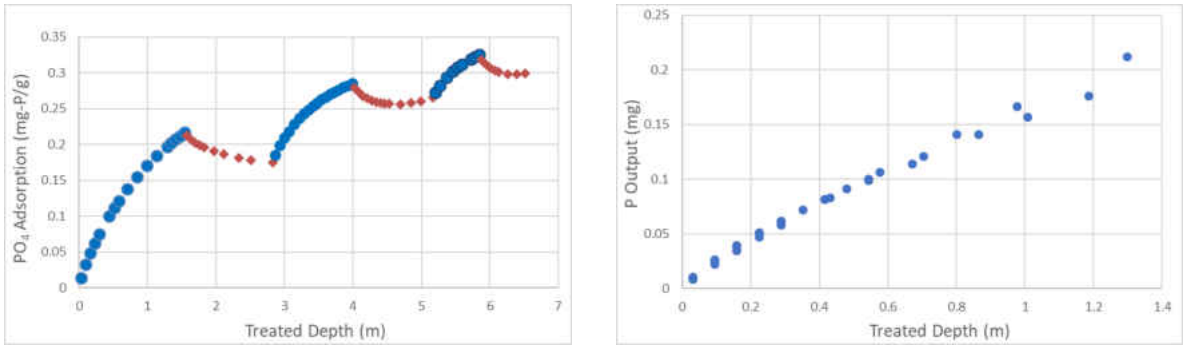


(A) (B)

FIGURE 6.14: Desorption reduction between cycles (A): cumulative mass retained (B): cumulative mass desorbed per cycle

## 6.6 Chapter Closing Remarks

This chapter presented the accumulated data analysis via residual P, cumulative mass retained, and multi-cycle plots to illustrate the P removal characteristics for an amended sand column. Residual P plots, in which the ordinates are directly collected from the experiment, is the basis upon integration to calculate the mass removed and retained from the column. Cumulative P retention is illustrated by the cumulative mass retained plots in which there exists a statistically significant trend between the amount

of amendment and P retained in column, there are no other parameters that demonstrate significance other than the pH. Desorption at the given conditions rendered a strong correlation between all $AlOH_3$ desorption events. Only, half a liter of influent is necessary to reduce the desorption removal efficiency to less than 20 percent. The multi-cycle plots distinguished the residual P plots with the mass retained plots. By visual inspection, less mass is retained in column when the area underneath the cycle in the residual P plot is smaller. More detailed results and analysis will be presented in the next section to draw systematic results and compare them with batch adsorption characteristics and literary studies. The following chapter will expound on the results above and quantify the column performance using known models and data from literary sources.

# Chapter 7

# DISCUSSION

## 7.1 Topics of Discussion

The previous chapters presented the data acquired from experimentation along with their results and basic analysis. This chapter will utilize the data to analyze, model, and extrapolate in order to quantify and compare the results to known models and methods presented in literature.

## 7.2 Batch Adsorption Isotherm Modeling

As discussed in the methodology chapter, the Freundlich and Langmuir models will be implemented to the aggregate isotherms of corresponding amendments and dosages to estimate the appropriate model in determining the peak adsorption capacities. The Freundlich equation represents a power function while the Langmuir mimics a comparable version of a logarithmic function. Each general model equation is applied to discover the equation parameter constants as tallied in Table 6.1. Although the Langmuir equation does not illustrate a $R^2$ value, by visual inspection it fits the $AlOH_3$ isotherms better, while the Freundlich model favors the $FeOH_3$ isotherms. The reasoning for this model bias is because the $FeOH_3$ isotherms still have increasing ordinates while

TABLE 7.1: Derived isotherm parameters for the Freundlich and Langmuir models

| **40 ppm Alum** | | | | | | |
|---|---|---|---|---|---|---|
| **Freundlich** ($C_s = K_f * C_w^n$) | | | | **Langmuir** ($C_s = S_{lm} * K_l * C_w/(1 + K_l * C_w)$) | | |
| *Parameter* | *Estimate* | *SE* | *R2* | *Parameter* | *Estimate* | *SE* |
| **Kf** | 0.54 | 0.073 | 0.42 | **Slm** | 0.937 | 0.122 |
| **n** | 0.273 | 0.084 | | **Kl** | 1.69833 | 0.980679 |
| **60 ppm Alum** | | | | | | |
| **Kf** | 0.860 | 0.046 | 0.71 | **Slm** | 1.340 | 0.096 |
| **n** | 0.251 | 0.037 | | **Kl** | 2.489 | 0.837 |
| **36.4 ppm Fe(Cl)3** | | | | | | |
| **Kf** | 1.11 | 0.187 | 0.78 | **Slm** | 7.167 | 2.484 |
| **n** | 0.577 | 0.095 | | **Kl** | 0.135 | 0.081 |
| **54.6 ppm Fe(Cl)3** | | | | | | |
| **Kf** | 1.631 | 0.159 | 0.82 | **Slm** | 5.986 | 1.080 |
| **n** | 0.499 | 0.064 | | **Kl** | 0.325 | 0.129 |

the $AlOH_3$ floc isotherm ordinates flatten out, rendering a better fit for the Langmuir model given its logarithmic nature. These models are represented as solid regression lines of their respective scatter plot aggregate isotherms in Figures 7.1 and Figures 7.2.

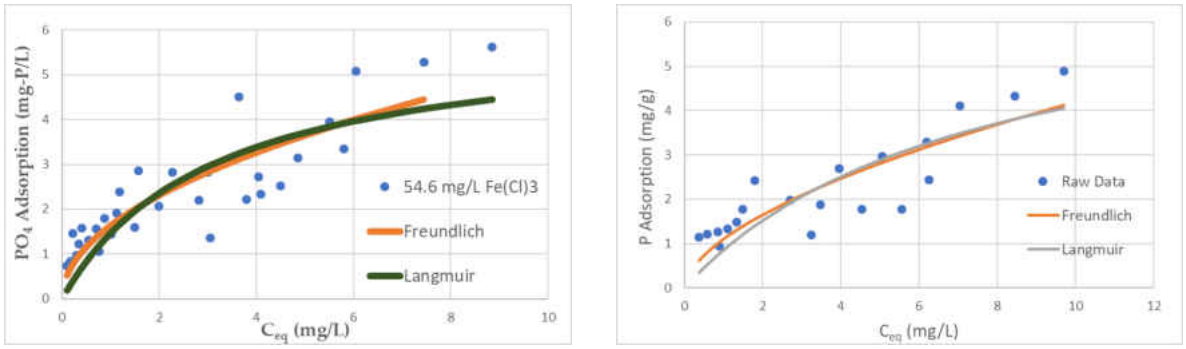


(A) (B)

FIGURE 7.1: $FeOH_3$ floc isotherm Freundlich and Langmuir models. (A): 54.6 mg/L isotherm data (B): 36.4 mg/L isotherm data

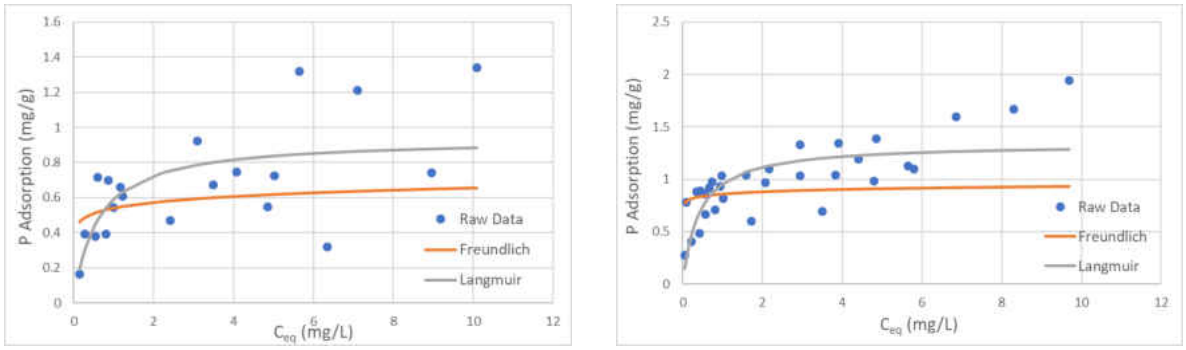


(A) (B)

FIGURE 7.2: $AlOH_3$ floc isotherm Freundlich and Langmuir Models. (A): 40 mg/L isotherm data (B): 60 mg/L isotherm data

### 7.2.1 Modeling Comparison with Previous Studies

It is implausible to estimate the peak adsorption using the Freundlich equation because its derivative is undefined as the function approaches zero (Figure E.1); although, the same incidence occurs for the Langmuir function, the peak adsorption value is much easier to estimate. Despite the fact the Freundlich model fits better for the $FeOH_3$ floc isotherm, the Langmuir model will be used to estimate the peak adsorption capacity (q) to be compared with column adsorption capacity and literature results.

An adequately large $C_{eq}$ is used as the predictor for the Langmuir models to discover q were the values are listed in Table 7.2. The results indicate that $FeOH_3$ floc has a substantially higher sorption potential than $AlOH_3$ floc. The $FeOH_3$ floc q suggest consistency with the Geolithe and Hematite adsorption capacity values in Table C.1. It appears as if the WTR floc contains a lesser capacity than some of the other materials listed in Table C.1, however, this study downplays the adsorption capacity of the inherent adsorbent (metallic (hydr)oxide), because the metallic (hydr)oxide contributes a miniscule amount of the entire WTR floc mass. Nonetheless it still represents the adsorption capacity of WTR, which is the relevant quantity if WTR is employed.

TABLE 7.2: Langmuir model: peak adsorption

| Peak adsorption | |
|---|---|
| Amendment (mg/L) | Peak Adsorption (mg/g) |
| $FeOH_3$ **floc** | |
| 36.4 | 7.114 |
| 54.6 | 5.97 |
| $AlOH_3$ **floc** | |
| 40 | 0.936 |
| 60 | 1.34 |

## 7.3 Cumulative P Mass Retention Discussion

Two types of adsorption methods are exploited to determine peak column adsorption capacity. The first method is coined empirical peak adsorption ($q_{emp}$), which involves the manipulation of the cumulative P retention data to determine the peak adsorption capacities by means of setting derivatives of the adsorption equations equal to zero to locate the TD at which the rate of adsorption is zero. The second method is called the Thomas Model ($q_{Thom}$), which is a widely accepted theoretical method to describe column adsorption performance. These values will be evaluated and compared with the batch reactor peak adsorption capacities as listed in Table 7.2 to observe how much the column factors inhibits P adsorption. In general, potentially the biggest factor dictating the adsorption capacity is the adsorption kinetics. Aforementioned, there are only a few second the adsorbate comes into contact with the adsorbent; therefore, less adsorption capacity is expected for the column experiments.

### 7.3.1 Empirical Peak Adsorption Capacity $q_{emp}$

As mentioned, this method is strictly empirical and is not a supported adsorption metric. Nonetheless, a relatively sound argument can be made to substantiate it's scientific

solidarity. The calculation initiates by integrating the residual P plot and dividing by the floc mass to achieve the adsorption at any given TD within the column. Sequentially, a second degree polynomial regression equation is extrapolated to the point at which the curve reverses. The peak of that curve is the the theoretical adsorption capacity ($q_{emp}$). To find this value, the derivative of the regression line is equated to zero and solved back to find the corresponding TD. That TD value can then by used in the polynomial regression equation to calculate the $q_{emp}$. Figure 7.3 displays the extrapolated adsorption curves to which the method is applied. Table 7.3 tabulates the $q_{emp}$ along with other relevant parameters.

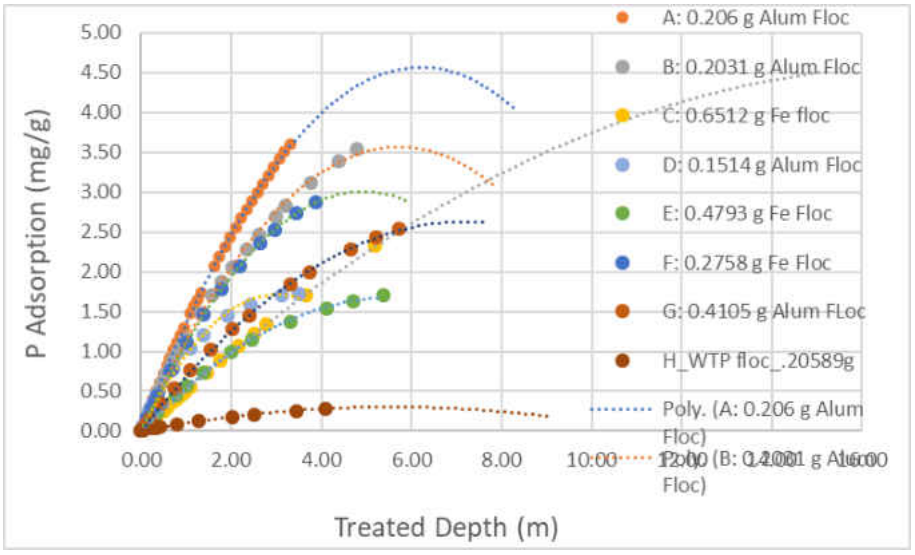


FIGURE 7.3: Cumulative P adsorption model for $q_{emp}$

To make the data in Table 7.3 meaningful, relationships can be made between each parameter to see if any statistically significant correlations exist. Table 7.4 presents a Spearman Rho correlation matrices that help discover and visualize the relationships between column parameters (see Figure E.2 for scatter plot matrices). The only strong

TABLE 7.3: Column parameters and empirical metrics derived from $q_{emp}$

| **Experiment** | **Flocculant** | **Floc Mass** | **ED** | $q_{emp}$ | **Peak Ret.** |
|---|---|---|---|---|---|
| A | Alum | 0.206 | 6.2 | 4.57 | 0.941 |
| B | Alum | 0.203 | 5.72 | 3.57 | 0.725 |
| C | Fe | 0.6521 | 17.58 | 4.61 | 3.006 |
| D | Alum | 0.1514 | 3.01 | 1.71 | 0.259 |
| E | Fe | 0.4705 | 5.56 | 1.67 | 0.786 |
| F | Fe | 0.2758 | 4.93 | 2.96 | 0.816 |
| G | Alum | 0.4105 | 7.23 | 2.63 | 1.080 |
| I | Alum | 0.1471 | 2.76 | 2.22 | 0.327 |
| J | Alum | 0.2577 | 1.66 | 0.82 | 0.211 |

TABLE 7.4: Spearman Rho column correlation parameter matrix: $q_{emp}$

| Floc Mass | Floc Mass | ED | $q_{emp}$ | Peak Retained |
|---|---|---|---|---|
| ED | 0.583 | | | |
| | 0.099 | | | |
| $q_{emp}$ | 0.183 | **0.767** | | |
| | 0.637 | **0.016** | | |
| Peak Retained | **0.667** | **0.917** | **0.75** | |
| | **0.05** | **0.001** | **0.02** | |
| Hydraulic loading | 0.051 | -0.221 | -0.383 | -0.111 |
| | 0.896 | 0.567 | 0.309 | 0.777 |
| pH | 0.13 | -0.484 | **-0.783** | -0.354 |
| | 0.738 | 0.186 | **0.013** | 0.35 |
| PO4 in | 0.143 | -0.059 | 0.034 | 0.168 |
| | 0.714 | 0.881 | 0.932 | 0.666 |

and statistically significant relationship that the floc mass has is with the peak retention value. Meaning, the more floc mass, the more P retained in the system. Surprisingly, there exists no statistically significant strong to moderate correlations between floc mass and exhaustion depth and the rest of the parameters. Some may be confounded why there is no correlation between the peak adsorption and floc mass, however this actually make sense because the characteristics of adsorption is not a function of quantity but quantity. Other relationships are indicated by boldface font such as the correlation between ED, and an excellent relationship with peak retained. This

indicates a larger amount of influent P solution to reach the peak P retention point. Peak adsorption also possesses a negative relationship with pH, meaning a higher pH diminishes the adsorption potential. As previously stated, this method is strictly empirical and has no scientific grounds for substantiation; therefore, the Thomas model adsorption results will help assess the reliability of this empirical method.

## 7.4 Thomas Model Analysis

The Thomas model is one of the more widely accepted theoretical methods to describe column adsorption performance. It assumes Langmuir kinetics of adsorption-desorption and derived with the assumption that the rate driving force obeys second-order reversible reaction kinetics (Thomas, 1944). This model will be compared with the extrapolated estimations of adsorption from the empirical method mentioned above and compared with the Langmuir batch adsorption capacities. Table 7.5 displays the equation parameters derived from the Minitab18 solver along with its corresponding Standard error (S). k represents Thomas rate coefficient (mL/mg/min) and $q_{Thom}$ represents the maximum adsorption capacity (mg/g). The plots can be viewed in Appendix E (Figures E.5-E.8). Overall, the model does a better job predicting the $q_{Thom}$ value than the k, which is fine because $q_{Thom}$ is the value of interest.

Table 7.6 is the correlation matrix relating the $q_{Thom}$ to the floc mass and pH, which illustrate similar relationships to the $q_{emp}$ relationships as previously shown (Table 6.4). Some of the parameters are excluded because ED and peak retained are parameters spurred from the empirical adsorption method rendering relationships between them and $q_{Thom}$ implausable.

TABLE 7.5: Thomas model: derived parameters

| Flocculant | Floc Mass | k | S estimate | $q_{Thom}$ | S estimate |
|---|---|---|---|---|---|
| Alum | 0.206 | 0.016 | 0.001 | 3.802 | 0.132 |
| Alum | 0.203 | 9.155 | 1.644 | 3.381 | 0.447 |
| Fe | 0.652 | 5.100 | 0.314 | 5.499 | 0.173 |
| Alum | 0.151 | 67.841 | 20.249 | 0.882 | 0.222 |
| Fe | 0.471 | 21.151 | 3.020 | 1.601 | 0.152 |
| Fe | 0.276 | 29.940 | 2.544 | 2.966 | 0.112 |
| Alum | 0.411 | 18.794 | 2.307 | 2.506 | 0.181 |
| Alum | 0.147 | 57.107 | 10.579 | 1.736 | 0.214 |
| Alum | 0.258 | 51.139 | 6.853 | 1.439 | 0.136 |

To compare the adsorption capacity methods, the $q_{Thom}$ and $q_{emp}$ ordinates were plotted at their shared floc mass to create a response curve (Figure 7.4(A)). Interestingly enough, the chart generates a strong linear 1:1 slope ratio, indicating that the two methods are relatively congruent, substantiating relative precision for both adsorption prediction methods. The standard error of regression tends to be greater on the data terminals and less for the central predictors as one can see when comparing the values in the adjacent figure (Figure 7.4(B)). The majority of points exist above the regression line indicating the empirical method exaggerates the adsorption capacity.

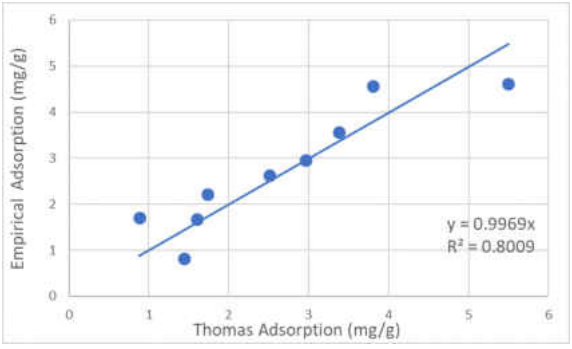


(A)

| Floc Mass | Thom. q | Empir. q |
|---|---|---|
| 0.2060 | 3.80 | 4.57 |
| 0.2031 | 3.38 | 3.57 |
| 0.6512 | 5.49 | 4.61 |
| 0.1514 | 0.88 | 1.71 |
| 0.4793 | 1.60 | 1.67 |
| 0.2758 | 2.96 | 2.96 |
| 0.4105 | 2.50 | 2.63 |
| 0.1477 | 1.73 | 2.22 |
| 0.2577 | 1.43 | 0.82 |

(B)

FIGURE 7.4: (A): Thomas model response curve. $R^2$= 0.8009, S= 0.5852. (B): Plot Values

TABLE 7.6: Spearman Rho correlation matrix: $q_{thom}$

| | Correlations | | |
|---|---|---|---|
| | Floc Mass | Thom. Q | pH |
| Thom. Q | 0.333 | | |
| | 0.381 | | |
| Influent pH | 0.13 | **-0.783** | |
| | 0.738 | **0.013** | |
| Hydr loading | 0.085 | -0.485 | **0.742** |
| | 0.828 | 0.186 | **0.022** |

## 7.5 Maximum Adsorption Summary

Now that all the maximum adsorption capacities of the column experiments have been determined, they can be compared with the batch adsorption capacities. Table 7.7 illustrates an average maximum adsorption capacity values ($q_{emp}$ and $q_{Thom}$) for each amendment in a distilled and surface water solution.

TABLE 7.7: Average adsorption capacities for amendments in distilled and surface water solution

| **Distilled Water** | | | | | |
|---|---|---|---|---|---|
| | | | $q_{Thom}$ave | | $q_{emp}$ave |
| aloh3 floc | 0.206 | 3.802 | | 4.57 | |
| aloh3 floc | 0.2031 | 3.381 | **3.592** | 3.57 | **4.07** |
| FeOH3 floc | 0.6512 | 5.499 | **5.499** | 4.61 | **4.61** |
| **Surface Water** | | | | | |
| | | | $q_{Thom}$ave | | $q_{emp}$ave |
| aloh3 floc | 0.1514 | 0.882 | | 1.71 | |
| Aloh3 floc | 0.4105 | 2.506 | | 2.63 | |
| Alum floc | 0.1477 | 1.736 | | 2.22 | |
| Alum floc | 0.2577 | 1.439 | **1.640** | 0.82 | **1.845** |
| FeOH3 floc | 0.4793 | 1.601 | | 1.67 | |
| FeOH3 floc | 0.2758 | 2.966 | **2.284** | 2.96 | **2.315** |

When comparing the batch adsorption capacities,its difficult to distinguish which model is better suited with the batch reactor adsorption capacity results as the column capacities heavily underwhelm the batch reactor $FeOH_3$ capacity, while th $AlOH_3$ floc

capacities are more compatible. There may be to many variables that occur in the column to render equivalent adsorption capacities, therefore there is no way to determine whether $q_{Thom}$ or $q_{emp}$ is the superior model.

## 7.6 Multi-cycle Column Experiment Discussion and Analysis

The multi-cycle adsorption experiments paint a better picture of column performance longevity. Figure 7.5 depicts the P retention multi-cycles plots while Table 7.8 tabulates the percent P retained after each cycle. It is quite clear the columns utilizing distilled water as the solution influent exhibited much better P retention, this is likely due to the an increased pH rather than the effects of sorption site competition which is consistent with the results from the single adsorption and batch reactor adsorption data. After two cycles 0.206 g $AlOH_3$ floc column retained 42.17 percent of all P influent, while 0.1477 g $AlOH_3$ floc column only retained 9.69 percent of influent P. This indicates the importance of pH and its effects on column adsorption.

TABLE 7.8: Percent retained per cycle

| Cycle | 0.1477 | 0.2577 | 0.206 | 0.203 |
|---|---|---|---|---|
| 1 cycle | 10.30 | 27.16 | 47.80 | 30.01 |
| 2 cycles | 9.69 | 22.47 | 42.17 | 23.50 |
| 3 cycles | 7.81 | 19.81 | | |

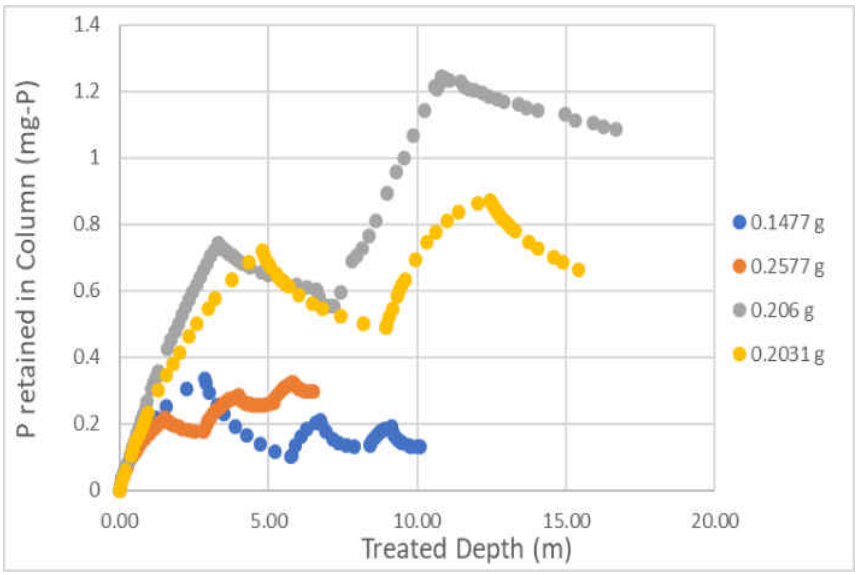


FIGURE 7.5: P retained multi-cycle plot comparison.

## 7.7 Final Remarks

Based off the literary comparison of different iron oxides, the adsorption capacity of $FeOH_3$ floc is similar to that of Geolithe and Hematite, which is impressive considering that the metallic (hydr)oxides is only a portion of WTR particle mass. $FeOH_3$ floc clearly outperformed the q of $AlOH_3$ floc in the column analysis and especially the batch adsorption analysis. The Freundlich isotherm model predicts the $FeOH_3$ isotherm better but the Langmuir model is more suitable for the $AlOH_3$ floc for the batch reactor studies were each model demonstrates strong to good fits that are statistically significant. Two methods were implemented to acquire q for the column experiments. $q_{emp}$, derived empirically, slightly overestimated the $q_{Thom}$ values derived from the Thomas model. The Spearman Rho correlation matrices indicated q is strongly influenced by the solution pH for both the models. The $q_{emp}$ is also highly

associated with the ED and Peak retained values.Finally, multi-cycle events using distilled solutions (lower pH) demonstrated a substantial increase in P retention were 0.206 and 0.203 retained 42.17 percent and 23.50 percent after two cycles, were columns with a surface water solution observed 7.81 and 19.81 percent retention.

# Chapter 8

# CONCLUSIONS

As bioretention and biofilters become an increasingly popular LID technique, better designs are needed to immobilize DP from stormwater. Without the use of DP capturing amendments, these LIDs are capable of releasing more P than is input. Amendments such as WTR are proven successful in capturing P to a relatively high degree. $FeOH_3$ floc according to the Langmuir isotherm model calculated an adsorption capacity of 7.114 mg-P/ g floc and 5.19 mg-P/ g floc for coagulant dosages of 36.4 mg/L and 54.6 mg/L respectively which renders a similar adsorption capacity to that of iron oxides: Geolithe and Hematite as indicated in Table C.1. While $AlOH_3$ floc exhibits less potential with adsorption capacities of 0.936 mg-P/g floc and 1.39 mg-P/g floc, they exhibit characteristics more alike $FeOH_3$ floc in the column experiments. The two methods for estimating adsorption potential in the column experiments, empirical and Thomas model, rendered values more conservative than the batch reactor models. The Thomas model estimated values even more conservative than the empirical values but both methods are in statistical agreement.

The primary component impacting P adsorption is the influent pH. A lower pH (<6) increases the adsorption capacity of the amendments, however 6-8 is the more realistic pH range that should be considered for engineering design. The short contact time between the runoff and amendments did not impact the adsorption potential as the outer-sphere complexation mechanisms required only seconds for completion, but left

the system susceptible to substantial desorption.

### 8.0.1 Potential Application

Hypothetically, lets say an engineer wants to design a bioretention cell to capture P for a 1 acre parking lot were 90 percent rainfall is converted to runoff. The average P concentration is 0.22 mg/L (Table B.1), the average yearly rainfall for the region is 20.57 inches. The adsorption capacity of the amendment is 2.315 mg-P/g floc. If the engineer use a 1:100 amendment to sand ratio. The floc adsorption capacity would not reach exhaustion for 488 years. However, this value is an exaggeration as crystallization, clogging, and bypassing traditionally transpires; secondly, the amendments are not completely efficient in adsorbing P as seen in Table 7.8. If the engineer decides to achieve a minimum 50 percent P removal efficiency, further calculations would have to ensue, reducing the BMP life span.

### 8.0.2 Implications

Although, the previous application indicates a significant life span, some caveats limit the design and usage of amended bioretention cells. micro flocs from water treatment facilities can clog media pores and substantially reduces the hydraulic conductivity, rendering the BMP unworkable because it cannot retain and filter runoff. Flocs accompanied with polymers demonstrate to substantially reduce adsorption capacities and should be avoided as amendments. The use of polymers is troubling because an

increasing number of WTP are implementing polymers to increase coagulation efficiency and reduce product costs, limiting numerous municipalities access to proper WTR bioretention amendments.

### 8.0.3 Closing Statements

As state and local authorities continue to recognize the detrimental effects of eutrophication upon sensitive water bodies due to excessive nutrient loading, they will be searching for inexpensive yet effective methods to mitigate eutrophic ramifications. Implementing WTR amendments to bioretention systems will be a progressively excellent option in capturing P from stormwater surface runoff as they have proven to be an innovative, low cost, and effective method in neutralize environmental footprints down to pre-developement levels.

# Appendix A

# LITERATURE REVIEW TABLES AND FIGURES

TABLE A.1: Equilibrium constants of orthophosphate species at 25 °C

| Chemical Equation | $pK_a$ |
|---|---|
| $H_3PO_4 = H^+ + H_2PO_4^-$ | 2.2 |
| $H_2PO_4^- = H^+ + HPO_4^{2-}$ | 7.2 |
| $HPO_4^{2-} = H^+PO_4^{3-}$ | 12.7 |

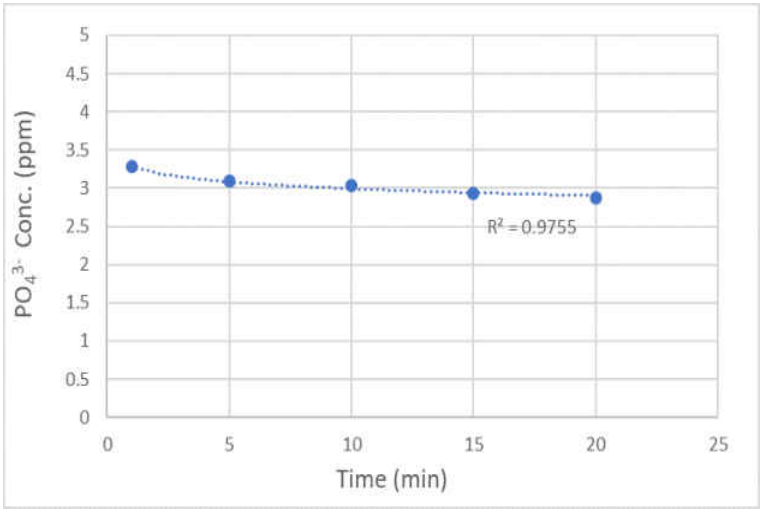


FIGURE A.1: Phosphate adsorption kinetics. S=0.0284 $R^2$= .9673, P= 0.002

# Appendix B

# COAGULATION MATRIX DISCUSSION: CHARTS AND FIGURES

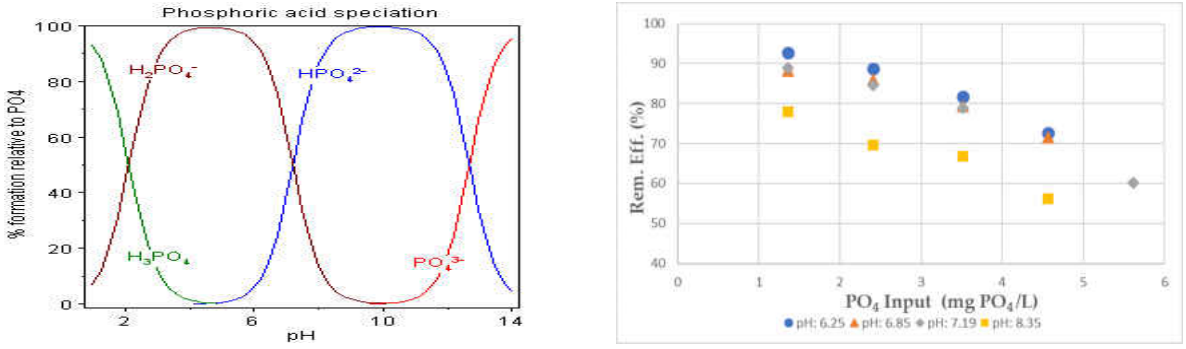


(A) (B)

FIGURE B.1: DP speciation and pH removal efficiency plot.(A) Phosphoric acid speciation ratio vs. pH. (B): Removal efficiency vs $PO_4$ input at varying pH

TABLE B.1: Average phosphorus concentrations per land use category

| Land Use | TP Concentration | | SRP Concentration | |
|---|---|---|---|---|
| | Median (mg/L) | Coefficient of Variation (unitless) | Median (mg/L) | Coefficient of Variation (unitless) |
| Residential | 0.30 | 1.1 | 0.17 | 0.9 |
| Commercial | 0.22 | 1.2 | 0.11 | 1.2 |
| Industrial | 0.26 | 1.4 | 0.11 | 1.2 |
| Institutional | 0.18 | 1.0 | 1.3 | 0.5 |
| Freeways | 0.25 | 1.8 | 0.20 | 2.1 |
| Open Space | 0.31 | 3.5 | 0.13 | 0.9 |

# Appendix C

# LOG-NORMAL PLOTS FOR BATCH ANALYSIS

TABLE C.1: Phosphate adsorption capacities of different iron oxides at pH 3.5

| Material | Chemical Formula | Capacity (mg-P/g) |
|---|---|---|
| Amorphous hydrous iron oxide (gel) | FeOOH | 29.5 |
| Akaganeite | $\beta$ – FeOOH | 26.7 |
| Lepidocrocite | $\gamma$ – FeOOH | 16.7 |
| Geothite | $\alpha$ – FeOOH | 6.7 |
| Hematite | $\alpha$ – $Fe_2O_3$ | 5.3 |
| Dry Tailings | 30% iron oxide | 8 |

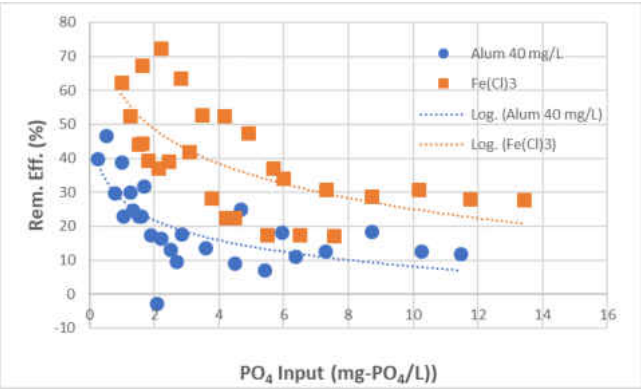


FIGURE C.1: Batch reactor aggregate removal efficiency. (A): 40 mg/L Alum (P=0.00) (B): 36.4 mg/L $FeCl_3$ (P=0.00)

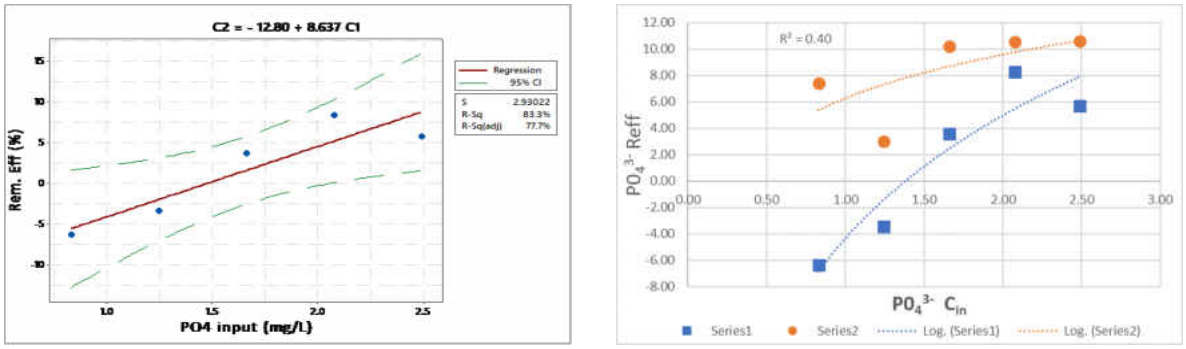


(A) (B)

FIGURE C.2: Supernatant adsorption batch experiment: removal efficiency plots (A): log-normal (B): No Outliers

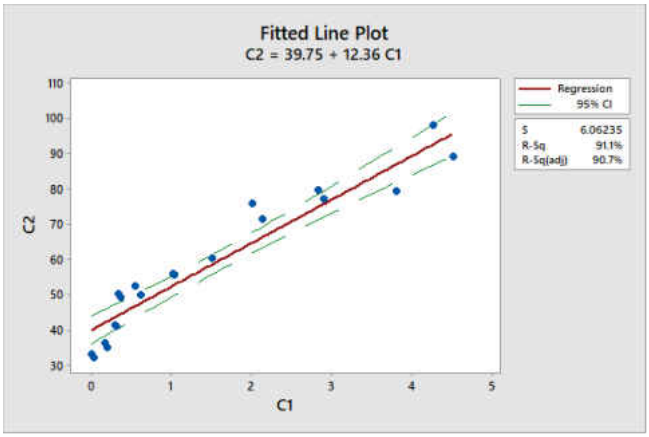


FIGURE C.3: Log-norm turbidity isotherm for Figure 5.2. S= 6.062, $R^2$= 0.911

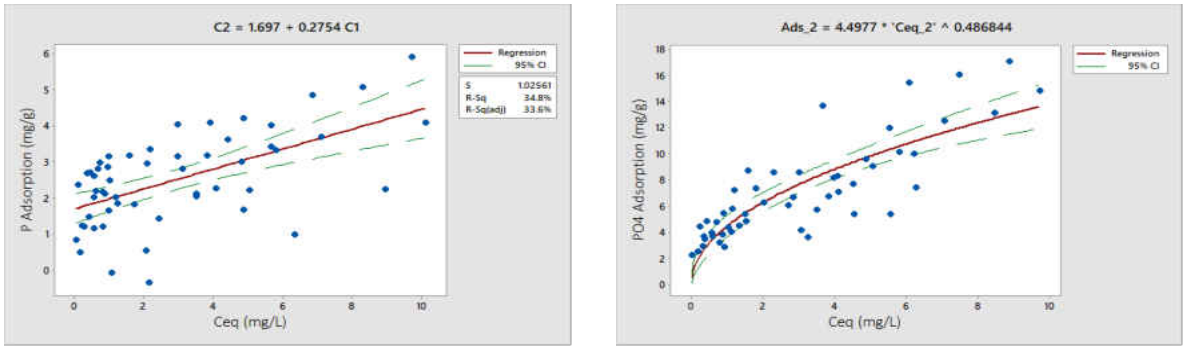


(A) (B)

FIGURE C.4: Aggregate isotherms (A): $AlOH_3$ floc: $R^2$= 34.81, S= 2.194, P=0.000 (B): $FeOH_3$ floc: $R^2$= 71.62, S= 2.03, P= 0.00

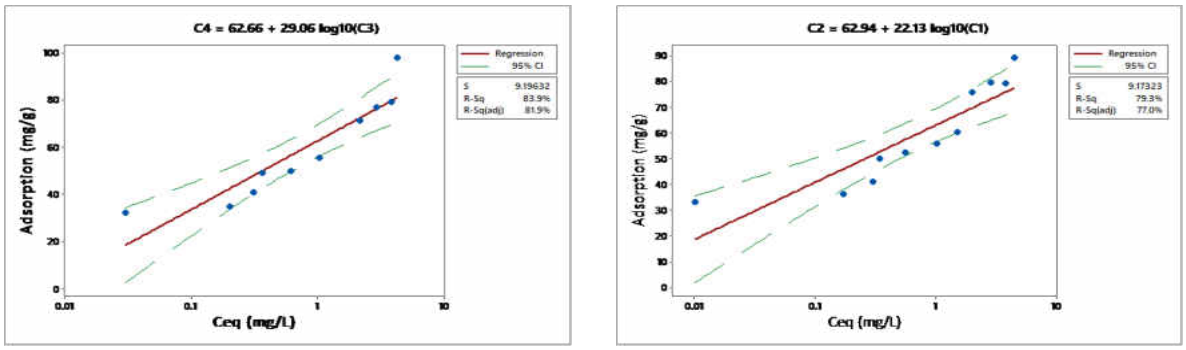


(A) (B)

FIGURE C.5: Turbidity test: log-normal isotherms. (A): S= 9.196, $R^2$= 0.839. (B): S= 9.173, $R^2$= 0.793

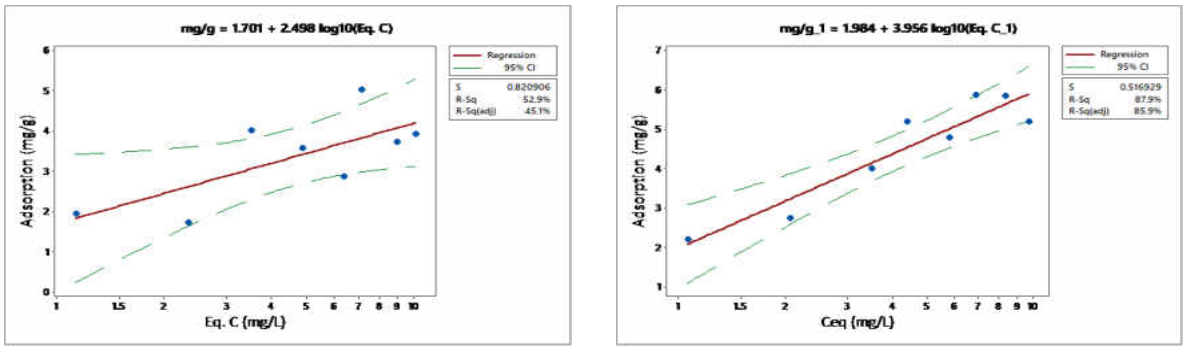


(A) (B)

FIGURE C.6: Log-normal isotherms for Figure 5.4(A). (A): S= 0.821, $R^2$= 0.529. (B): S= 0.517, $R^2$= 0.879

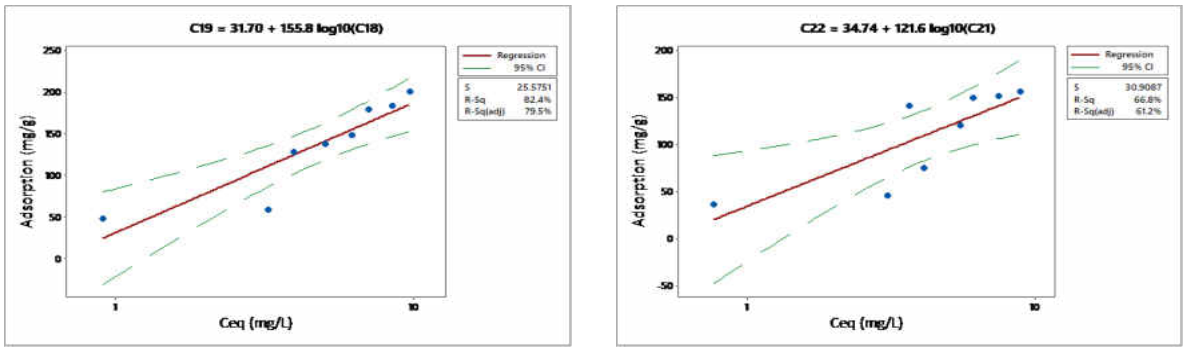


(A) (B)

FIGURE C.7: Log-norm isotherms for Figure 5.4(B). (A): S= 25.575, $R^2$= 0.824 (B): S= 30.909, $R^2$= 0.668

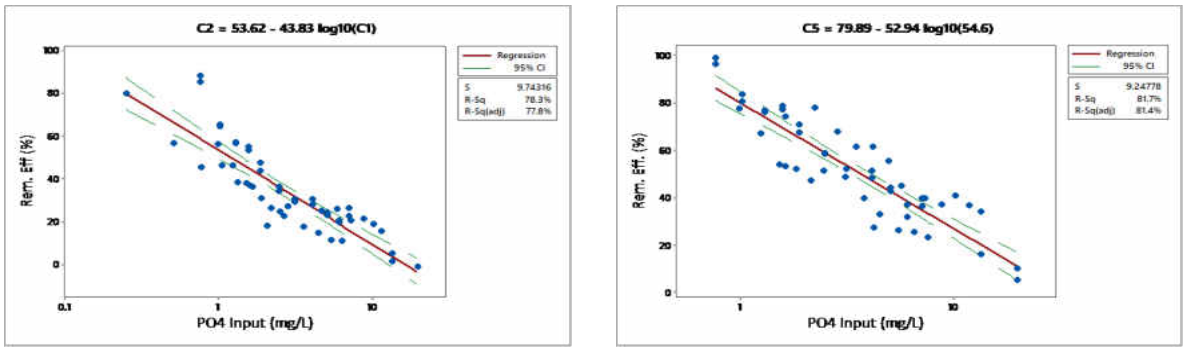


(A) (B)

FIGURE C.8: Log-normal removal efficiency plots for Figure 5.5. (A): 60 mg/L alum. S= 9.74, $R^2$= 0.783, P= 0.000 (B): 54.6 mg/L $FeCl_3$. S= 9.248, $R^2$= 0.818, P= 0.000

TABLE C.2: Amorphous versus Aged Floc Adsorption Performance:

| Coagulant | floc Mass(g) | $PO_4$Out |
|---|---|---|
| Dry Alum | 0.0756 | 0.54 |
| Amorphous Alum | 0.0752 | 0.81 |
| WTP Alum | 0.0755 | 0.915 |
| Amorphous WTP Alum | 0.0758 | 1.59 |

# Appendix D

## COLUMN RESULTS AND FIGURES

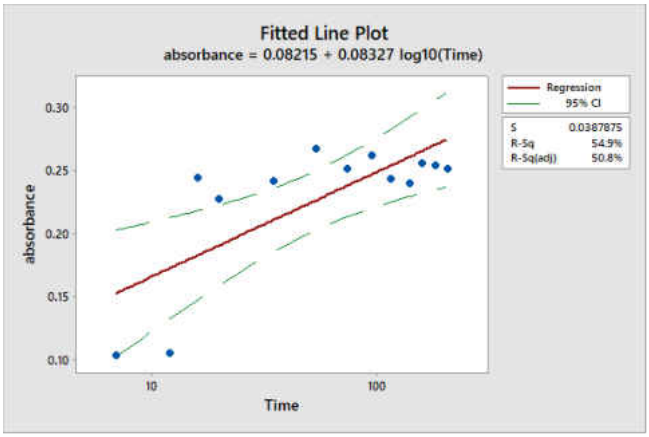


FIGURE D.1: Log-normal NOM plot S= 0.039, $R^2$= 0.549

TABLE D.1: 1 L correlation matrix

| | mass | Rate | pH | P in |
|---|---|---|---|---|
| Rate | 0.085 | | | |
| | 0.828 | | | |
| pH | 0.13 | 0.742 | | |
| | 0.738 | 0.022 | | |
| P in | 0.305 | 0.727 | 0.36 | |
| | 0.425 | 0.026 | 0.341 | |
| 1 L | 0.733 | -0.043 | -0.261 | 0.424 |
| | 0.025 | 0.913 | 0.498 | 0.256 |

TABLE D.2: 2 L correlation matrix

| | Mass | Rate | pH | P in |
|---|---|---|---|---|
| Rate | 0.085 | | | |
| | 0.828 | | | |
| pH | 0.13 | 0.742 | | |
| | 0.738 | 0.022 | | |
| P in | 0.305 | 0.727 | 0.36 | |
| | 0.425 | 0.026 | 0.341 | |
| 2 L | 0.717 | -0.111 | -0.354 | 0.373 |
| | 0.03 | 0.777 | 0.35 | 0.323 |

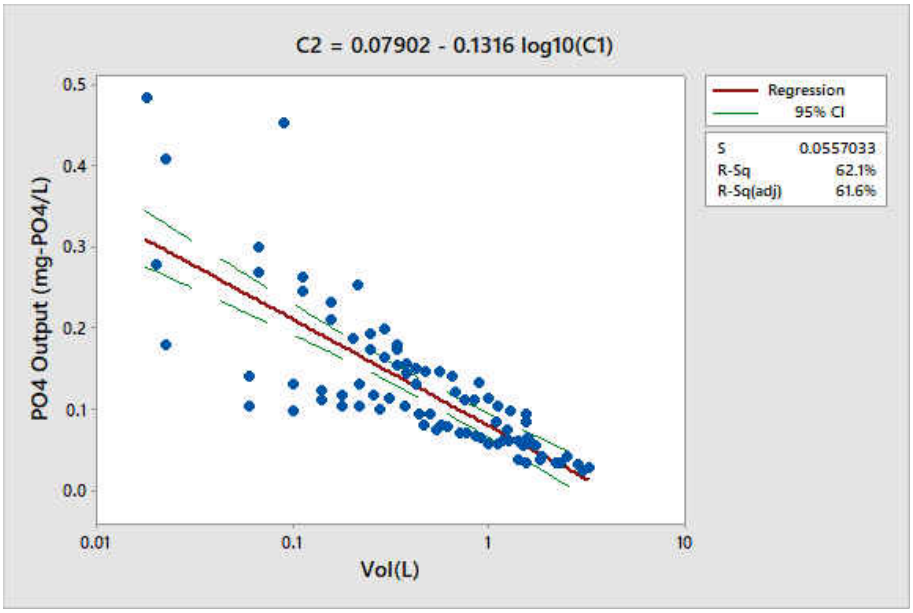


FIGURE D.2: Aggregate desorption log-normal plot for Figure 6.7(B). S= 0.056, $R^2$= 0.621

| Lack of Fit Summary for Column Tests | | | | | | | | | |
|---|---|---|---|---|---|---|---|---|---|
| **Test** | **0.4105** | **0.4758** | **0.2758** | **0.1514** | **0.6512** | **0.2301** | **2.06** | **0.1477** | **0.2577** |
| **Iterations** | 9 | 11 | 6 | 2 | 12 | 2 | 2 | 2 | 2 |
| **Final SSE** | 0.010342 | 0.011136 | 0.010057 | 0.043796 | 0.020135 | 0.009616 | 0.010269 | 0.011031 | 0.008376 |
| **DFE** | 12 | 12 | 11 | 10 | 29 | 20 | 8 | 9 | 15 |
| **MSE** | 0.000862 | 0.000928 | 0.000914 | 0.00438 | 0.000694 | 0.000481 | 0.001284 | 0.001226 | 0.000558 |
| **S** | 0.029356 | 0.030463 | 0.030237 | 0.066179 | 0.02635 | 0.021927 | 0.035827 | 0.03501 | 0.02363 |

FIGURE D.3: Lack of fit summary for column analysis

# Appendix E

## DISCUSSION ANALYSIS: TABLES AND FIGURES

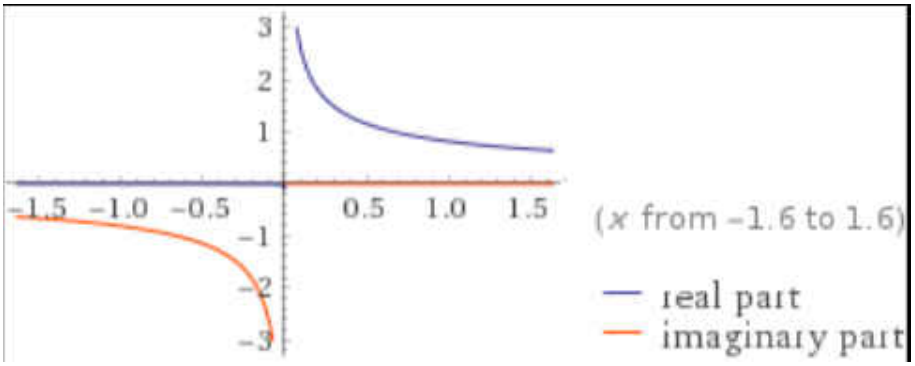


FIGURE E.1: Freundlich derivative equation for 54.6 mg/L $FeOH_3$ floc

FIGURE E.2: Removal efficiency plot summary

| | P Removal Efficiency (%) vs. Treated Depth | | | | | | | | | | |
|---|---|---|---|---|---|---|---|---|---|---|---|
| | A (.206 g Alum Floc) | B (.2031 Alum Floc) | B cycle 2 | D (.1514 Alum floc) | C (.6512 g FeOH3 floc) | E (.4793 g FeOH3 floc) | F .2758 g( FeOH3 Floc) | G (.4105 g Alum Floc) | H (2.0589 g WTP alum floc) | I(.1477 g Alum) | J (.2577 g Alum ) |
| R2 | 0.9642 | 0.904 | 0.9215 | 0.7535 | 0.9597 | 0.956 | 0.9564 | 0.8732 | 0.9808 | | |
| T.D | | | | | | | | | | | |
| 0 | 100.00 | 100.00 | 100.00 | 100.00 | 100.00 | 100.00 | 100.00 | 100.00 | 100.00 | 100.00 | 100.00 |
| 0.25 | 84.44 | 76.74 | 71.41 | 50.27 | 96.88 | 84.37 | 92.74 | 86.94 | 66.67 | 63.07 | 60.90 |
| 0.5 | 77.94 | 69.09 | 61.89 | 40.56 | 94.77 | 76.85 | 86.89 | 80.73 | 59.25 | 48.86 | 45.88 |
| 0.75 | 72.95 | 63.50 | 54.91 | 34.01 | 92.93 | 70.87 | 81.47 | 75.81 | 54.17 | 40.55 | 37.09 |
| 1 | 68.73 | 58.93 | 49.20 | 28.94 | 91.23 | 65.71 | 76.32 | 71.57 | 50.18 | 34.65 | 30.86 |
| 1.25 | 65.02 | 54.99 | 44.27 | 24.74 | 89.64 | 61.09 | 71.36 | 67.78 | 46.85 | 30.08 | 26.02 |
| 1.5 | 61.66 | 51.50 | 39.90 | 21.12 | 88.13 | 56.86 | 66.54 | 64.31 | 43.96 | 26.34 | 22.07 |
| 1.75 | 58.56 | 48.33 | 35.93 | 17.93 | 86.69 | 52.92 | 61.84 | 61.09 | 41.40 | 23.18 | 18.73 |
| 2 | 55.68 | 45.42 | 32.28 | 15.06 | 85.29 | 49.22 | 57.24 | 58.06 | 39.09 | 20.44 | 15.84 |
| 2.25 | 52.98 | 42.72 | 28.89 | 12.44 | 83.94 | 45.71 | 52.72 | 55.20 | 36.98 | 18.03 | 13.29 |
| 2.5 | 50.42 | 40.19 | 25.72 | 10.03 | 82.63 | 42.37 | 48.28 | 52.47 | 35.02 | 15.87 | 11.00 |
| 2.75 | 47.98 | 37.81 | 22.72 | 7.80 | 81.35 | 39.18 | 43.90 | 49.86 | 33.20 | 13.91 | 8.94 |
| 3 | 45.65 | 35.55 | 19.88 | 5.71 | 80.10 | 36.10 | 39.58 | 47.35 | 31.49 | 12.13 | 7.05 |
| 3.25 | 43.42 | 33.40 | 17.18 | 3.74 | 78.87 | 33.14 | 35.31 | 44.94 | 29.89 | 10.49 | 5.32 |
| 3.5 | 41.27 | 31.35 | 14.59 | 1.89 | 77.67 | 30.27 | 31.09 | 42.60 | 28.36 | 8.97 | 3.71 |
| 3.75 | 39.19 | 29.37 | 12.11 | 0.13 | 76.49 | 27.49 | 26.91 | 40.34 | 26.92 | 7.56 | 2.22 |
| 4 | 37.18 | 27.48 | 9.73 | -1.54 | 75.33 | 24.79 | 22.78 | 38.14 | 25.54 | 6.23 | 0.82 |
| 4.25 | 35.24 | 25.66 | 7.43 | -3.14 | 74.19 | 22.16 | 18.68 | 36.00 | 24.21 | 4.99 | -0.50 |
| 4.5 | 33.35 | 23.89 | 5.21 | -4.67 | 73.06 | 19.60 | 14.62 | 33.91 | 22.95 | 3.82 | -1.73 |
| 4.75 | 31.51 | 22.19 | 3.06 | -6.14 | 71.96 | 17.10 | 10.59 | 31.88 | 21.73 | 2.71 | -2.91 |
| 5 | 29.72 | 20.53 | 0.98 | -7.55 | 70.86 | 14.66 | 6.60 | 29.89 | 20.56 | 1.66 | -4.02 |

FIGURE E.3: Column Experiments scatter plot matrix

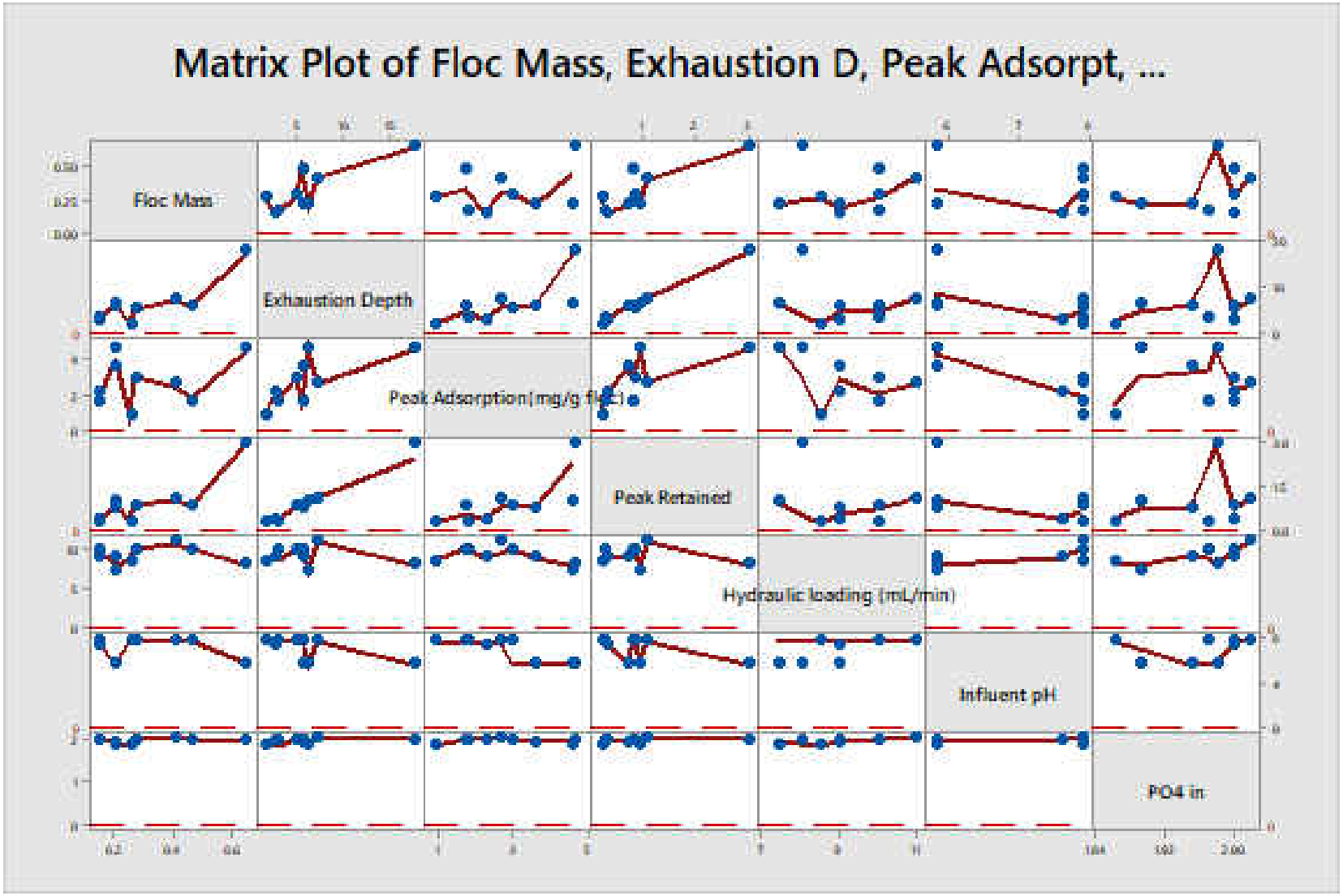

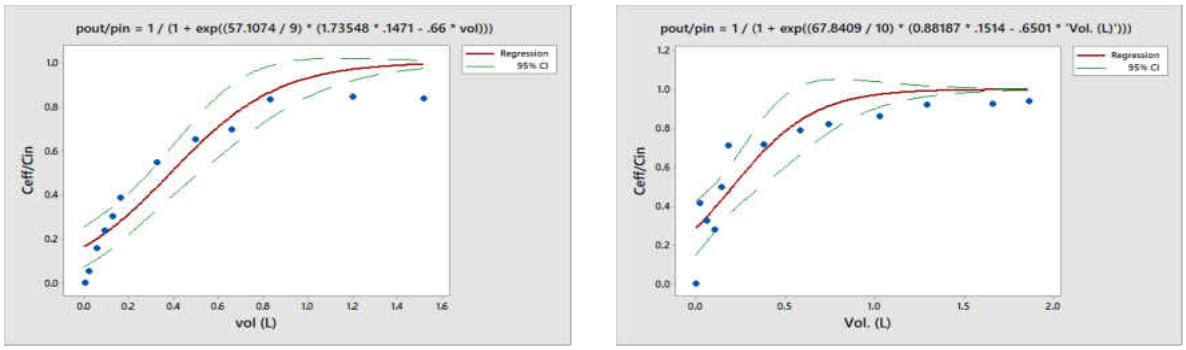


(A) (B)

FIGURE E.4: (A):0.1471g & (B): 0.1514 g Thomas Models

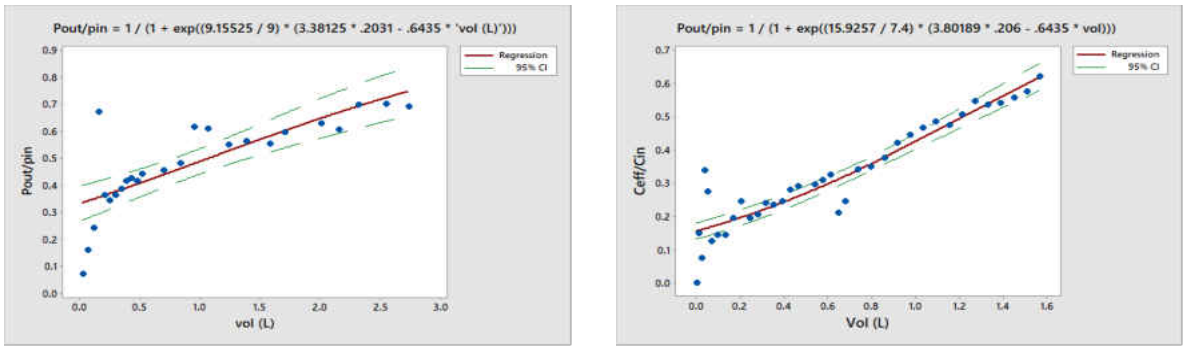


(A) (B)

FIGURE E.5: (A): 0.2031 g & (B): 0.2060 g Thomas Models

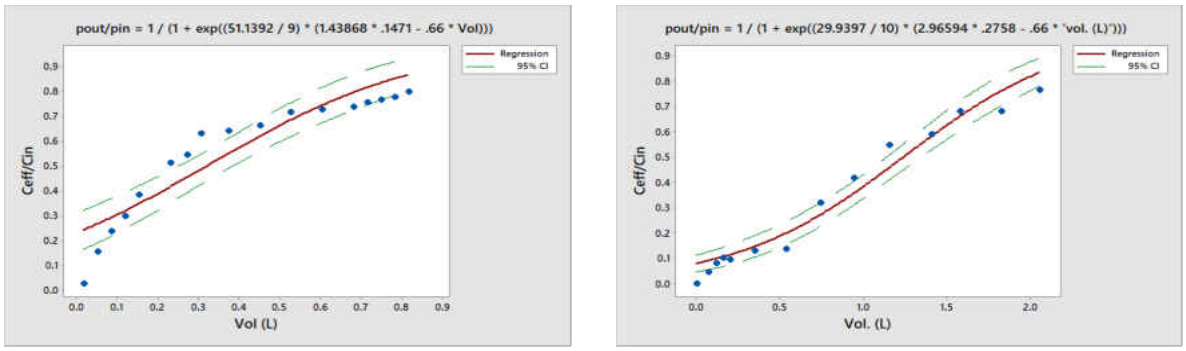


(A) (B)

FIGURE E.6: (A): 0.2577g & (B): 0.2758 g Thomas Models

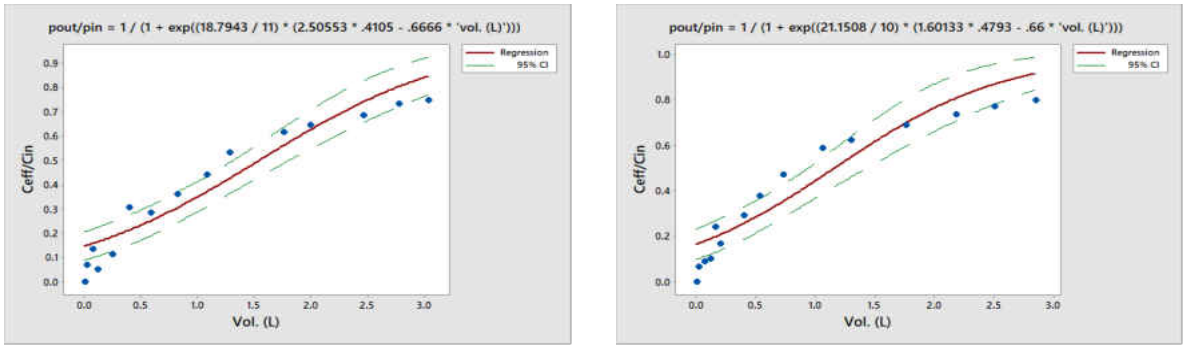


(A) (B)

FIGURE E.7: (A): 0.4105g & (B): 0.4705 g Thomas Models

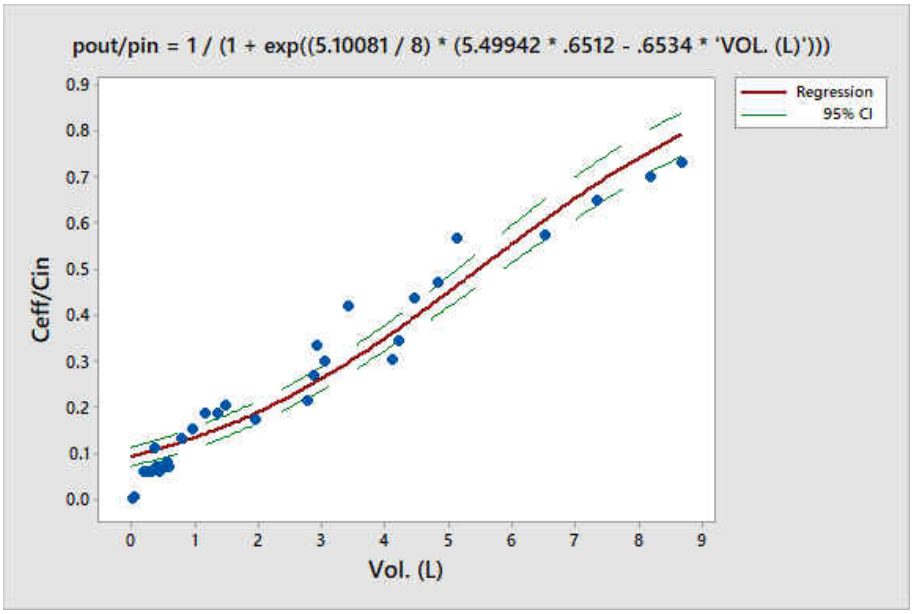


FIGURE E.8: 0.6521 g Thomas Model

## REFERENCES

A. Ghribi and M. Chlendi, 2011. Modeling of Fixed Bed Adsorption: Application to the Adsorption of an Organic Dye. Asian Journal of Textile, 1: 161-171.

Berkowitz, J., Anderson, M. A., & Amrhein, C. (2006). Influence of aging on phosphorus sorption to alum floc in lake water. Water Research, 40(5), 911-916. doi:10.1016/j.watres.2005.12.018

Bolan, N. S. (1991). A critical review on the role of mycorrhizal fungi in the uptake of phosphorus by plants. Plant and Soil, 134(2), 189-207. doi:10.1007/bf00012037

Cordell, D.; Drangert, J. O.; White, S. Global Environmental Change. 2009, 19, 292–305.

Corbridge, D.E.C. 2000. Phosphorus 2000. In Chemistry, Biochemistry and Technology. Elsevier, Amsterdam, The Netherlands.

Council, N. R.; National Academies Press: 2009. Davis, A. P., Hunt, W. F., Traver, R. G., & Clar, M. (2009). Bioretention Technology: Overview of Current Practice and Future Needs. Journal of Environmental Engineering, 135(3), 109-117. doi:10.1061/(asce)0733-9372(2009)135:3(109)

Davis, A. P., and McCuen, R. H. (2005). Stormwater management forsmart growth, Springer, New York.

Erickson, A. J., Gulliver, J. S., & Weiss, P. T. (2012). Capturing phosphates with iron enhanced sand filtration. Water Research, 46(9), 3032-3042. doi:10.1016/j.watres.2012.03.009

Fertilizer usage data. http://www.epa.gov/nutrient-policy-data/commercial-fertilizer-purchased #table2

Griffin, R. A., & Jurinak, J. J. (1973). The Interaction of Phosphate with Calcite1. Soil Science Society of America Journal, 37(6), 847. doi:10.2136/sssaj1973.03615995003700060018x

Hathaway, J., Brown, R., Fu, J., & Hunt, W. (2014). Bioretention function under climate change scenarios in North Carolina, USA. Journal of Hydrology, 519, 503-511. doi:10.1016/j.jhydrol.2014.07.037

Health, N. D. D. o. North Dakota 2014 Integrated Section 305(b) Water Quality Assessment Report and Section 303(d) List of Waters Needing Total Maximum Daily Loads, 2014. Iqbal, H., Garcia-Perez, M., & Flury, M. (2015). Effect of biochar on leaching of organic carbon, nitrogen, and phosphorus from compost in bioretention systems. Science of The Total Environment, 521-522, 37-45. doi:10.1016/j.scitotenv.2015.03.060.

Kayhanian, M., C. Suverkropp, A. Ruby and K. Tsay, 2007. Characterization and Prediction of HighwayRunoff Constituent Event Mean Concentration, Journal of Environmental Management, 85: 279-295

J Stewart, Russell & C Ransom, Todd & Hlady, Vladimir. (2011). Natural Underwater Adhesives. Journal of polymer science. Part B, Polymer physics. 49. 757-771.

10.1002/polb.22256.

Lefevre, G. H., Paus, K. H., Natarajan, P., Gulliver, J. S., Novak, P. J., & Hozalski, R. M. (2015). Review of Dissolved Pollutants in Urban Storm Water and Their Removal and Fate in Bioretention Cells. Journal of Environmental Engineering, 141(1), 04014050. doi:10.1061/(asce)ee.1943-7870.0000876

Lewitus, A. J., Brock, L. M., Burke, M. K., Demattio, K. A., & Wilde, S. B. (2008). Lagoonal stormwater detention ponds as promoters of harmful algal blooms and eutrophication along the South Carolina coast. Harmful Algae, 8(1), 60-65. doi:10.1016/j.hal.2008.08.012

Li, J., & Davis, A. P. (2016). A unified look at phosphorus treatment using bioretention. Water Research, 90, 141-155. doi:10.1016/j.watres.2015.12.015

Lucke, T., & Nichols, P. W. (2015). The pollution removal and stormwater reduction performance of street-side bioretention basins after ten years in operation. Science of The Total Environment, 536, 784-792. doi:10.1016/j.scitotenv.2015.07.142

Maestre, A., and Pitt, R. (2005). "The National Stormwater Quality Data-base, Version 1.1 a compilation and analysis of NPDES stormwatermonitoring information."U.S. Environmental Protection Agency(EPA) Office of Water, Washington, DC.

Mangangka, I. R., Liu, A., Egodawatta, P., & Goonetilleke, A. (2015). Performance characterisation of a stormwater treatment bioretention basin. Journal of Environmental Management, 150, 173-178. doi:10.1016/j.jenvman.2014.11.007

Masters, G. M.; Ela, W. Introduction to Environmental Engineering and Science; 3rd ed.; Prentice Hall: Upper Saddle River, N.J., 2008.

Miller, R. W.; Donahue, R. L.; Miller, J. U. Soils : An introduction to soils and plant growth; 6th ed.; Prentice-Hall International: London, 1990.

Mullane, J. M., Flury, M., Iqbal, H., Freeze, P. M., Hinman, C., Cogger, C. G., & Shi, Z. (2015). Intermittent rainstorms cause pulses of nitrogen, phosphorus, and copper in leachate from compost in bioretention systems. Science of The Total Environment, 537, 294-303. doi:10.1016/j.scitotenv.2015.07.157

Parfitt, R. L., R. J. Atkinson, and R. St.C. Smart. 1975. The Mechanism of Phosphate Fixation by Iron Oxides1. Soil Sci. Soc. Am. J. 39:837-841. doi:10.2136/sssaj1975.03615995003900050017x

Roy-Poirier, A., Champagne, P., & Filion, Y. (2010). Bioretention processes for phosphorus pollution control. Environmental Reviews, 18(NA), 159-173. doi:10.1139/a10-006

Sø, H. U., Postma, D., Jakobsen, R., & Larsen, F. (2011). Sorption of phosphate onto calcite; results from batch experiments and surface complexation modeling. Geochimica et Cosmochimica Acta, 75(10), 2911-2923. doi:10.1016/j.gca.2011.02.031

Stumm, W., and Morgan, J. J. (1981). Aquatic chemistry: An introductionemphasizing chemical equilibria in natural waters, Wiley, New York.

Snoeyink, V. L.; Jenkins, D. Water Chemistry; Wiley: New York, 1980.

Thomas, H.C., 1944. Heterogeneous ion exchange in a flowing system. J. Am. Chem. Soc., 66: 1664-1666.

Tonolla, D., Bruder, A., & Schweizer, S. (2017). Evaluation of mitigation measures to reduce hydropeaking impacts on river ecosystems – a case study from the Swiss Alps. Science of The Total Environment, 574, 594-604. doi:10.1016/j.scitotenv.2016.09.101

USEPA Nutrient Effects on Aquatic Ecology, Recreation and Drinking Water Supply: Nutrient and Key Response Indicators New Orleans, LA, 2011.

Yagi, S., & Fukushi, K. (2012). Removal of phosphate from solution by adsorption and precipitation of calcium phosphate onto monohydrocalcite. Journal of Colloid and Interface Science, 384(1), 128-136. doi:10.1016/j.jcis.2012.06.063

Zeng, L., Li, X., & Liu, J. (2004). Adsorptive removal of phosphate from aqueous solutions using iron oxide tailings. Water Rese